# Nitrogen-Doped Char as a Catalyst for Wet

# **Oxidation of Phenol Contaminated Water**

Iva Tews<sup>1</sup>, Aidan Garcia<sup>2</sup>, Michael Ayiania<sup>1</sup>, Sohrab Haghighi Mood<sup>1</sup>, Kalidas Mainali<sup>1</sup>,

Jean-Sabin McEwen<sup>1, 2, 3, 4, 5</sup> and Manuel Garcia-Perez<sup>1, 6</sup>

<sup>1</sup>Department of Biological Systems Engineering, Washington State University, Pullman, WA 99164, USA

<sup>2</sup>Gene and Linda Voiland School of Chemical Engineering and Bioengineering, Pullman, WA 99164, USA

<sup>3</sup>Department of Physics and Astronomy, Washington State University, Pullman, WA 99164

<sup>4</sup>Department of Chemistry, Washington State University, Pullman, WA 99164 <sup>5</sup>Institute for Integrated Catalysis, Pacific Northwest National Laboratory, Richland, WA, 99352

<sup>6</sup>Bioproducts Science and Engineering Laboratory, Richland, WA 99354

(Paper to be submitted to Biomass Conversion and Biorefinery)

Abstract: Catalytic wet oxidation (CWO) of aqueous effluents rich in organic compounds is a very promising technology for the treatment of liquid wastes from biomass conversion processes. CWO reactions occur through the formation of free radical species, produced in the presence of an oxidant, which act on organic contaminates in the effluent. Although the reaction is well known, there exists a lack of affordable catalysts to conduct this process at the lower temperatures and pressures in novel bioenergy processes. This study assessed the catalytic effect of nitrogen-doped chars as such an option. Phenol in aqueous solution was used as a model waste effluent. Treatment was conducted at moderate temperatures (190 to 260 °C), oxygen partial pressure of 1 MPa, and reaction times of 15, 30, and 45 min in stainless steel and glass-lined tube reactors. High pressure liquid chromatography (HPLC) analyses of the products quantified phenol and byproduct concentrations used in the calculation of reaction activation energy. The char catalyst was studied by X-ray Photoelectron Spectroscopy (XPS), Transmission Electron Microscopy (TEM) and Scanning Electron Microscopy (SEM) in order to gain insight into its structure and surface composition. The results indicate that nitrogen-doped char catalysts accelerate the oxidation of phenol by decreasing its reaction activation energy from 82.2 kJ/mol (noncatalyzed) to 40.4 kJ/mol (catalyzed). An analysis from first principles using Density Functional Theory (DFT) was conducted to ascertain which N functional group have the most significant impact on free radical formation in the presence of oxygen. Among all the N functional groups studied the di-pyridinic functional groups showed the most promising characteristics to facilitate the formation of hydroxyl free radicals.

Keywords: Nitrogen doped chars; Phenol oxidation; Oxidation kinetics

\*Corresponding author:

Manuel Garcia-Perez

Professor

Department of Biological Systems Engineering,

2710 Crimson Way

Washington State University

Richland, Washington, 99354-1671

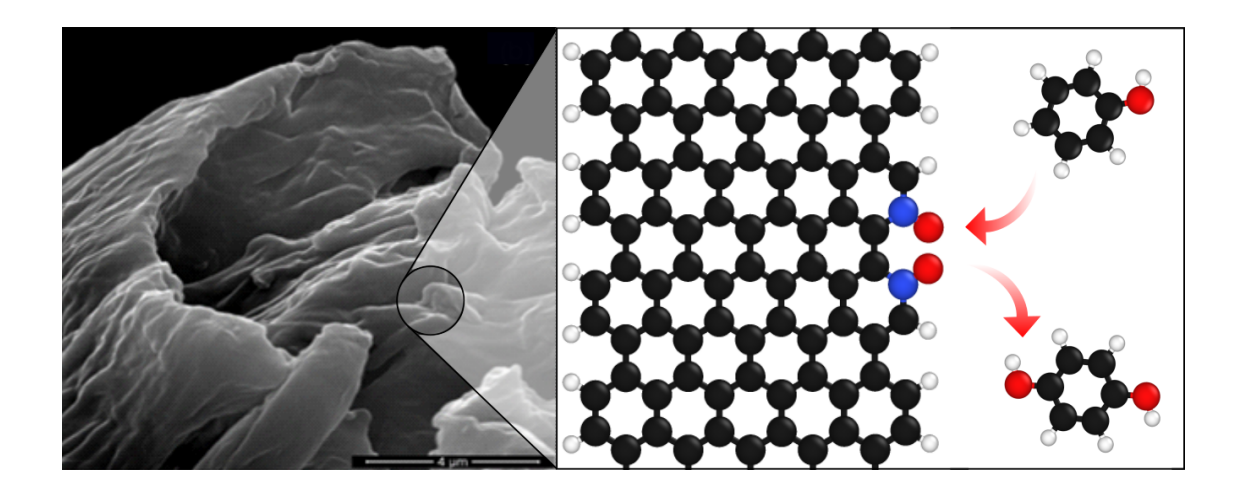
Phone number: 509-372-7461

e-mail: mgarcia-perez@wsu.edu

## **Highlights:**

- Available treatment of phenol contaminated water is reviewed, and active carbons are
  proposed as an inexpensive and robust solution to the shortcomings of existing
  catalysts.
- Nitrogen doped char, produced from cellulose, is a sustainable and affordable catalyst for adsorption and removal of phenol from water.
- Pyridinic groups comprise the highest percentage of functional groups in N-doped char.
- Density Functional Theory analysis confirms that in the presence of oxygen, pyridinic groups favorably produce activated oxygen species which are key to catalytic oxidation of phenol in water.

# **Graphical Abstract:**



### 1. Introduction

Aqueous effluent from various chemical industries contain significant amounts of toxic and refractory organic compounds. Many thermochemical processes utilizing wood or woody wastes produce an aqueous effluent with phenolic compounds (phenols, 2chloropheol, p-nitrophenol, o-cresol) at concentrations between 500 and 1000 ppm (Panisko et al., 2015; Tanksale et al., 2010; Villegas et al., 2016, Petersen, 1984). Concentrations of phenols between 9 and 25 ppm are generally considered toxic for humans and aquatic life (Villegas et al., 2016; Kulkarni et al. 2013). A recent review on phenol toxicity by Duan et al (2018) reported values of the median aquatic lethal concentrations (LC50) and the median effect concentration (EC50) for phenol, m-cresol and pcresol between 0.26 and 1204 ppm. Clearly the level of toxicity of phenols depend on the molecule structure and the micro-organism studied. The current EPA regulations set the maximum phenol contamination of less than 2 ppm in drinking water and 1 ppb in surface water (Villegas et al. 2016; Agency for Toxic Substances and Disease Registry 2018). Removal of phenols is by no means a new effort, and oxidation reaction studies specifically targeting phenol contaminated water have been researched and published for several decades (Devlin & Harris, 1984b; Djeffal et al., 2014; Grant & King, 1990; Kolaczkowski et al., 1999; Miguelez et al., 1997; F. J. Rivas et al., 1998). However, the bioenergy industry has stimulated a renewed effort in the treatment of aqueous effluents with highly dilute phenol concentrations (He et al., 2020; Wilson et al., 2019).

Catalytic Wet Oxidation (CWO), a type of Advanced Oxidative Process (AOP) has shown promise in the treatment of industrial aqueous wastes rich in organic compounds (Bhargava et al., 2006; Villegas et al., 2016). Carried out in the presence of an oxidant such as ozone, high pressure oxygen, and a catalyst, CWO of organic compounds typically occurs in two stages: (1) Physical Stage: transfer of oxygen from the gas phase to the liquid phase, and (2) the Chemical Stage: formation of free radicals and their reaction with an organic compound. One of the first complete mechanisms of phenol oxidation with dissolved oxygen was proposed by Devlin and Harris in 1984, making it clear that many intermediates can form in the oxidation process (Devlin & Harris, 1984). More detailed chemical reaction kinetics of the second stage were proposed by Rivas et al. developing a wet air oxidation mechanism driven by oxygenated free radicals (F. J. Rivas et al., 1998). To achieve complete phenol removal from aqueous effluents, stronger oxidants such as

ozone and hydrogen peroxide, alone or in the presence of metal catalysts, were introduced into the CWO process (F.J. Rivas et al., 1999). Homogeneous catalysts such Cu(NO<sub>3</sub>)<sub>2</sub>, heterogeneous inorganic metal catalyst such as Ru/C and Ru-Ce/C, as well as oxides such as CuSO<sub>4</sub> and MnO<sub>2</sub> have all shown to be efficient wet oxidation catalysts and effectively remove phenol at moderate temperatures and pressures (Bhargava et al., 2006; Kolaczkowski et al., 1999; F. J. Rivas et al., 1999; Rodríguez-Ramos et al., 2002). However, the use of strong oxidizers is inordinately expensive, and metal catalysts are prone to leaching toxic end products (Kolaczkowski et al., 1999). While altering the supports for existing catalysts has mitigated this (Liotta, Gruttadauria, Di Carlo, Perrini, & Librando, 2009), these challenges may be better addressed with more robust non-metal catalysts.

Activated carbons (ACs) have long been applied as inexpensive filtration adsorbents in wastewater treatment (Bhargava et al., 2006). More recently, ACs produced from waste materials such as anaerobically digested fiber, rice straw and woody wastes, referred to as chars or bio-chars, are being developed as catalytically active nanomaterials (Goran et al., 2015; Liu et al. 2019, Mood et al., 2020). Like activated carbon, chars contain intersecting graphitic layers, each consisting a honeycomb of carbon atoms (Estrade-Szwarckopf, 2004). These layers can contain nitrogen and other heteroatomic defects, allowing for tunable surface chemistry (Blume et al., 2015; Estrade-Szwarckopf, 2004; Yang et al., 2020; Zhang et al., 2013). Notable applications of these engineered carbonaceous materials include heterogeneous catalysts and adsorbents for pollutants such as H<sub>2</sub>S and CO<sub>2</sub> (Adib et al., 2000; Ayiania, Carbajal-Gamarra, et al., 2019; Chen et al., 2013; Mood et al., 2020; Nandi et al., 2012).

The use of active carbons in catalytic wet oxidation of phenol is not new and was well described by Santiago *et al.* 2005 (Santiago, Stüber, Fortuny, Fabregat, & Font, 2005). However, nitrogen doping – the act of introducing nitrogen groups in carbonaceous materials – has been shown to result in novel adsorptive and catalytic capabilities (Ding et al., 2020) not yet applied to CWO of phenol (Ayiania, Carbajal-Gamarra, et al., 2019; Mood et al., 2020; Z. Sun et al., 2019). Among these are inexpensive and highly active oxidative catalysis thought to benefit from the improved electron donor/acceptor capability of nitrogen functionalities present on the catalyst surface (Krasheninnikov & Nieminen, 2011). As such, nitrogen doped chars are of high interest as replacement for their pure

carbon counterparts, especially in the case of CWO processes (Ding et al., 2020; Liu et al., 2019).

This publication is focused on the development, characterization, and analysis of the catalytic effect of nitrogen-doped char on the wet oxidation of phenol. Cellulose char was used as a clean support material for the nitrogen doping such that no impurities could contribute to the catalytic activity. The char was characterized by SEM, TEM and XPS analysis. Catalytic activity of the char was assessed through development of Arrhenius kinetic parameters based on the change of phenol concentration present in the water under various oxidative conditions. To better understand which nitrogen functionality had the most significant impact on the oxidation of phenol, a Density Functional Theory (DFT) analysis was also conducted.

### 2. Materials and Methods

#### 2.1. Catalyst production

The nitrogen doped char was produced through slow carbonization of cellulose fibers produced by Fluka Analytica, Ireland (Avicel® PH-101, Lot #BCBG9043V) followed by ammonization at a temperature of 850 °C. Flow rates of 500 mL min<sup>-1</sup> for N<sub>2</sub> and 1000 mL min<sup>-1</sup> for ammonia gas were employed. This was conducted in a Quartz Tube furnace reactor with 50 mm OD by 44 mm ID at a length of 1000 mm. The carbonization was conducted under an oxygen free atmosphere by purging the reactor with N<sub>2</sub> gas. Briefly, cellulose fibers were kept in a tubular furnace in contact with N<sub>2</sub> for 30 min at 25 °C. Then, the temperature was increased from 25 °C to the desired set temperature of 850 °C at a heating rate of 10 °C min<sup>-1</sup>. The reactor was then kept at the set temperature for 2 h. After the first hour, the sample was treated with ammonia gas for 1 h. The final char produced was cooled down to 25 °C under N<sub>2</sub> gas before storage and utilization. Similar conditions are used by other researchers in the production of nitrogen doped char (Ding et al., 2020; Wan *et al.*, 2020). Control cellulose char was produced in the same method described above using identical cellulose fibers by Fluka Analytica, Ireland (Avicel® PH-101, Lot #BCBG9043V) however with only carbonization at 850 °C.

In order to evaluate the performance of our N-doped char we conducted comparative studies with a known oxidation catalysts (CuSO<sub>4</sub>). The Copper (II) Sulfate Pentahydrate control catalyst (CuSO<sub>4</sub>) was produced by Sigma-Aldrich St. Louis, MO (Lot#

#### MKBD8735V).

#### 2.2. Analysis of resulting carbon

The proximate composition of the N-doped char studied (moisture, fixed carbon, volatiles, and ash) was determined by using a thermogravimetric analyzer (TGA) SDTA851e (Mettler-Toledo, USA) according to ASTM standards E 871, E 1755, and E872 and Garcia et al. (2013). The elemental composition (CHNS-O) of the N-doped char was carried out using a TRUSPEC-CHN® (LECO, St. Joseph, MI, USA) elemental analyzer. The surface area was measured via CO<sub>2</sub> and N<sub>2</sub> physisorption with the aid of micromeritics TriStar II PLUS Surface Area and Porosity Analyzer (Norcross, GA, USA). While CO<sub>2</sub> adsorption isotherms were determined at 273 K, N<sub>2</sub> adsorption isotherms were measured at 77 K. Surface elemental composition was measured by X-ray photoelectron spectroscopy (XPS) using an AXIS-165 (Kratos Analytical Inc. Manchester, UK) with Achromatic X-ray radiation of 1253.6 eV (MgKα). The deconvolution process of the XPS char data was developed in an in-house excel based routine. In order to better tune the fitting parameters, such as the asymmetry factor, the asymmetric tailing factor (TL), and the G-L (Gaussian-Lorentzian ratio) as well as the FWHM custom calculations were produced and coded. The asymmetry factor was allowed to relax in the range of 0-0.20, the G-L ratio in the range of 0-0.30 and FWHM in the range of 1.4-2.0. Scanning electron microscope (SEM) imaging analysis was carried out using Hitachi S-570 variable pressure instrument. Transmission electron microscopy (TEM) was carried out using a FEI Tecnai G2, FEI Company (Field Emission Instruments).

#### 2.3. Wet oxidation

Phenol from Sigma Aldrich (NY) was used as a model molecule to study oxidation reactions. It was dissolved in e-pure water produced by the Barnsted E-Pure water filtration system to form solutions containing 1000 ppm [1000 mg/L]. Oxidation reactors were custom designed utilizing stainless steel tubes of 0.5 in O.D. and a total reactor volume of 28 mL. A glass sleeve insert was designed with a total volume 12 mL and used in all but the initial reactions. Each reactor was assembled with a sanitary fitting and coupling, swage lock fittings and a stainless-steel integral bonnet needle valve for both gas inlet and outlet as well as pressure release (Fig. 1). *Reactor assembly:* Each reactor housed one glass sleeve with 10 g of phenol aqueous sample would be pressurized to 1 MPa with nitrogen for control studies or pure oxygen for oxidation studies. For catalytic wet oxidation reactions,

0.2 wt% char catalyst would first be placed in the glass sleeve followed by introduction of the 10 g of phenol aqueous sample, vigorous mixing to suspend the solids, and gas pressurization. Reactions took place in an excess of oxidant at all times. A TECHNE Industrial Fluidized sand bath was used for heat transfer to the three reactors operating in parallel, at temperature ranging from 190 to 260 °C. Isothermal experiments were conducted for a total of 15, 30 to 45 minutes.



Figure 1. Stainless steel reactor schematic.

The content of phenol and secondary intermediate hydroquinone (Sigma Aldrich, Raleigh, NC, USA) in the liquid products of wet oxidation was quantified by high-pressure liquid chromatography. Briefly, a 10 μL injection of each sample was made onto an Aminex HPX- 87H ion exclusion column, (Bio-Rad), 300 mm long, 7.8 mm inner diameter. The column was equipped with a 30 mm long by 4.6 mm inner diameter guard column, using a Varian HPLC system. The column was eluted isocratically with 0.005 M sulfuric acid through an ultraviolet (UV) detector. The UV detector operational temperature was set at 65 °C. Calibration curves were developed for phenol obtained by Sigma-Aldrich (99% purity). Curves were obtained through four-point calibrations with a range of 1000 ppm to 10 ppm (1000 mg/L to 10 mg/L).

#### 2.4. Kinetic study

An important step in oxidative reactions is the formation of hydroxyl radicals which can be generated by the presence of oxygen, ozone, or catalysts. One of the first studies of this kinetic step and the decomposition mechanism dates back to 1964. In this study, the authors found that iron salts and ozone produce hydroxyl radicals (Eisenhauer, 1964, 1971). Since then, Kolaczkowski *et al.* (1999), among many, have further developed the understanding of oxidative reaction kinetics with respect to phenol. In general phenol oxidation reaction rate is expressed as follows:

$$-r_{Ph} = \frac{dC_{Ph}}{dt} = k_{Ph,O_2} \cdot C_{Ph}C_{O_2}$$
 (1)

where,  $C_{Ph}$  and  $C_{O_2}$  denote the concentration of phenol and oxygen in the liquid phase, respectively, and  $k_{Ph,O_2}$  represents the rate constant. In the literature, it has been widely reported that the phenol reaction order is one (Pruden and Le 1976; Miguelez *et al.* 1997; Kolaczkowski *et al.* 1999). This makes  $\alpha$  in Equation 1 equal to one and simplifies the expression. In order to study this reaction, the tests are conducted in excess of oxygen (at a high partial pressure of  $O_2$ ), so that for practical purposes its concentration in the liquid remains almost constant through the experiments. The integral form of Eq. 1 becomes,

$$ln\left(\frac{C_{Ph}}{C_{Ph_0}}\right) = k't \tag{2}$$

$$k' = k_{Ph,O_2} C_{O_2} = A e^{-\frac{E}{RT}} \cdot C_{O_2}$$
 (3)

where, k' is the pseudo first order rate constant [s<sup>-1</sup>], A the pre-exponential factor [s<sup>-1</sup>], and E is the activation energy [kJ mol<sup>-1</sup>]. In this study, these integrated kinetic expressions were used to fit experimental data and estimate activation energy values that were subsequently used to evaluate the catalytic activity of the N-doped chars.

## 2.5. Density Functional Theory (DFT) Analysis

The suitability of different active sites for oxidation was assessed using the Vienna abinitio Simulation Package (Joubert, 1999; Kresse & Furthmüller, 1996; Kresse & Hafner, 1993). A Perdew-Burke-Ernzerhof (PBE) functional was used to simulate valence electrons, with spin polarization enabled to account for the paramagnetic nature of oxygen species tested (Perdew et al., 1996). The core electrons were modelled using a projector augmented wave (updated 2015) with a plane wave energy cutoff of 450 eV. Gaussian smearing of 0.2 eV was utilized to ease Brillouin integration convergence, and force

tolerance of 0.02 eV/ Å used as structural relaxation criteria. The energy tolerance was set to  $10^{-5}$  eV.

Sites tested were broadly grouped into carbonaceous, pyridinic (6-membered N), pyrrolic (5-membered N), and graphitic (N within the graphene sheet) functionalities. Graphene nanoribbons with hydrogen terminated edges (29×17×21 Å) were used for most active sites, and a pristine graphene sheet (14.8×14.8×20 Å) was used for internal defects (Ayiania, Hensley, et al., 2019). In the graphene nanoribbon model, the layer to layer distance in the supercell is 17 Å, and the graphene lattice constant is 2.467 Å. Illustrations and examples of models used in our calculations are shown in the supporting information (SI). Brillouin Integration was conducted over a  $(1\times1\times2)$  Monkhorst-Pack grid for nanoribbons and a (3×3×1) Monkhorst-Pack for pristine sheets, in order to minimize interactions between individual sheets and ribbons through the periodic boundaries (Monkhorst & Pack, 1976). Reactants were modelled in the gas phase using an 18×19×20 Å box and one single k-point (the Gamma point) to span the Brillouin zone. Sites were tested for their ability to adsorb and activate oxygen by relaxing adsorbates on the surface to establish bound energies. Resulting energies were then compared to the bare surface and gas-phase oxidants to produce binding energies. The adsorption energy of O<sub>2</sub> on the tested models are defined as:

$$E_{\rm ads} = E_{\rm O_2(ads)} - (E_{\rm surf} + E_{\rm O_2(g)})$$
 (4)

where  $E_{O_2(ads)}$ ,  $E_{surf}$ ,  $E_{O_2(g)}$  denote the calculated energies for an adsorbed  $O_2$  molecule on the N-doped sheet, the bare N-doped sheet and an  $O_2$  molecule in the gas phase. An analogous formula was used for the adsorption energy of an  $H_2O$  molecule.

A differential charge analysis was performed to obtain  $\Delta \rho$ : the net electronic exchange upon adsorption. The value of  $\Delta \rho$  was calculated using the equation below:

$$\Delta \rho = \rho_{\text{total}} - \rho_{\text{gas}} - \rho_{\text{surface}} \tag{5}$$

where  $\rho_{\rm total}$ ,  $\rho_{\rm surface}$  and  $\rho_{\rm gas}$  represent the charge distribution for the adsorbed system (surface with adsorbates present), the clean surface (the H-edged N-doped graphene sheet or the pure N-doped graphene sheet), and the gas phase molecule, respectively. We note that when calculating  $\rho_{\rm surface}$  and  $\rho_{\rm gas}$  the species are fixed in the same position as they

are found when the gas phase species adsorbs on the N-doped graphene sheet. As such, since the  $O_2$  molecule dissociates during adsorption, the amount of charge transfer does not necessarily correlate with its adsorption energy with respect to the intact  $O_2$  molecule in the gas phase. However, we include such an analysis since it is a useful assessment of chemical vs. hydrogen bonding. This is indicated in the charge analysis by a marked reduction in charge density corresponding to the cleavage of a shared Pi bond, even relative to the  $O_2$  molecule in its physically activated form.

#### 3. Results and discussion

#### 3.1. Production and Characterization of Carbonations Materials

To best understand the effect of the N-doped char on catalytic wet oxidation of aqueous phenol, several chars were developed with varying concentrations of nitrogen using ammonia as the nitrogen precursors. Char produced with no nitrogen under the same conditions was used as a control. Production and characterization of the various chars has been published by Ayiania et al. (2019, 2020).

Based on the initial screening of N-doped catalysts produced at various temperatures, and the analysis of these samples conducted by Ayiania et al. (2020), the char produced with ammonia precursors at 850 °C yielded a high surface area of 1305 m²/g under nitrogen (N₂) atmosphere and 1030 m²/g under carbon dioxide (CO₂). This is a significant improvement over the control cellulose char surface area of 705 m²/g (under CO₂). The slight discrepancy between the N₂ and CO₂ values can be explained by the fact that carbon dioxide adsorption is more effective in accurately estimating the micropores (0 to 2 nm). Nitrogen adsorption estimates both micropores and mesopores (2 to 50 nm), however it is more effective at estimating mesopores. For these reasons both N₂ and CO₂ adsorption isotherm and pore size distribution curves are given below.

Proximate analysis of the N-doped char indicated that 96.4 wt% of the carbon is fixed, with the rest of the mass accounting for volatiles as no ash is present. Ultimate analysis showed that 87.1 wt % was Carbon, 5.6 wt% Nitrogen, 0.8 wt% H and 6.5 wt% oxygen (by difference). The properties of the control char were not examined as a part of this study, but Muley et al. have completed an extensive review of cellulose char under similar conditions (Muley et al., 2016).

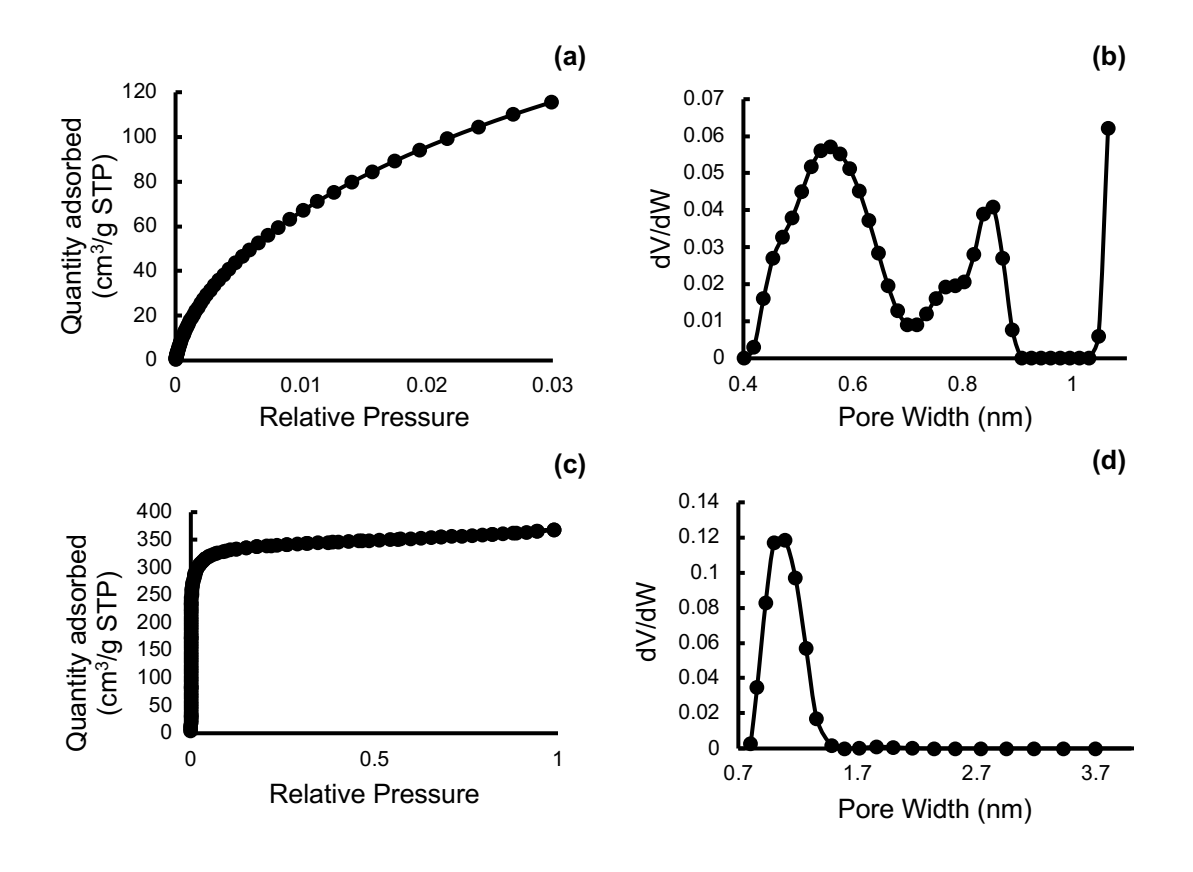


**Figure 2.**  $CO_2$  (a,b) and  $N_2$  (c, d) adsorption isotherm of char produced at 850 °C indicating pore development under ammonia conditions

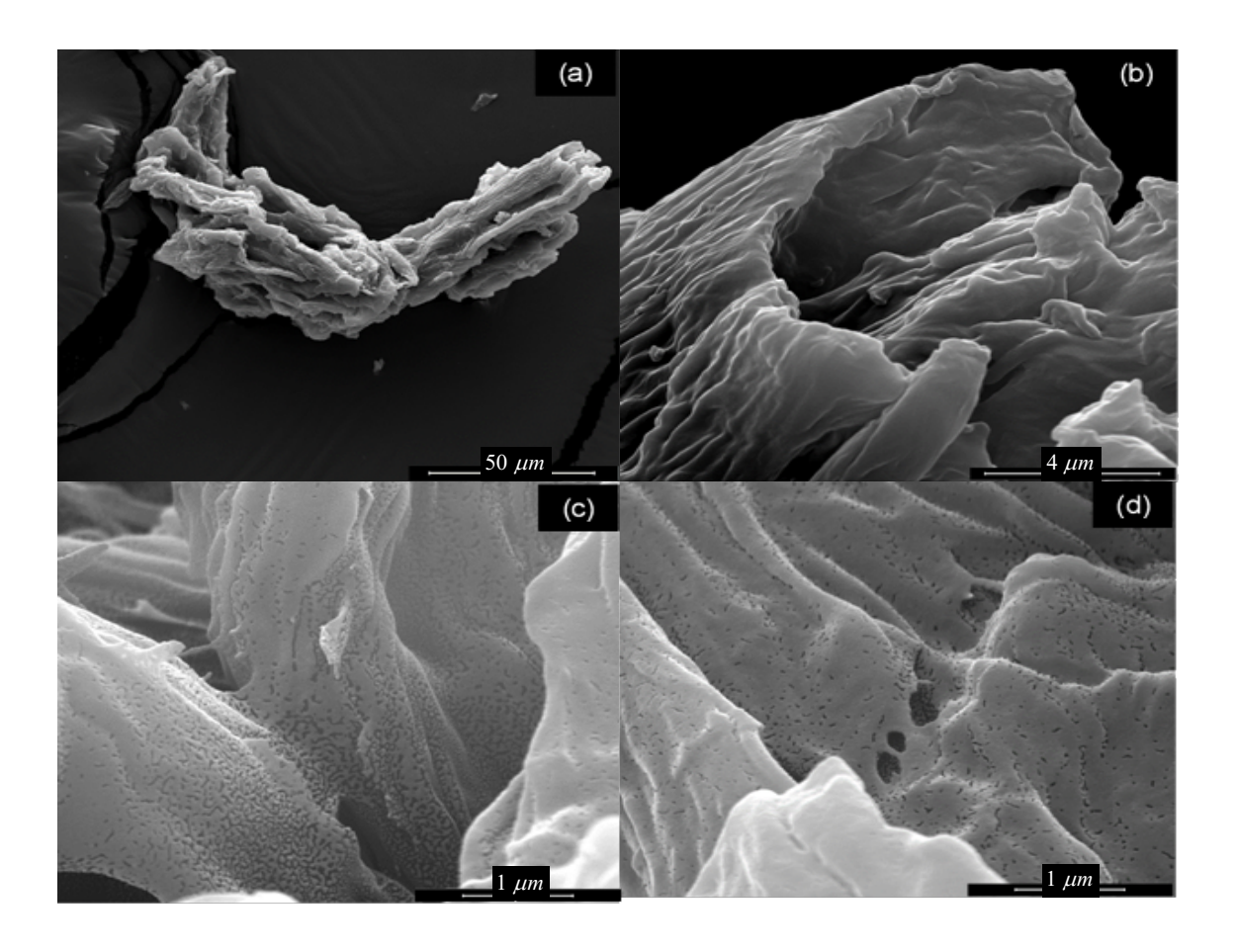


**Figure 3.** SEM images of nitrogen doped cellulose char pores contributing to high surface area and the efficacy as catalyst.

The surface area and pore size distribution produced by this method compares well with the literature (Luo et al., 2014; F. Sun et al., 2016). Luo *et al.* (2014) specifically studied the pyrolysis of cellulose under ammonia gas, and large surface areas were obtained at high temperatures of 850 °C and 1000 °C, closely mirroring the results presented here. Further understanding of the char morphology and microstructure was obtained through Scanning

Electron Microscopy (SEM) and Transmission Electron Microscopy (TEM) analysis, respectively. The SEM images (1,500 - 50,000x) seen in Fig. 3a and b shows the presence of channels and macro-pores. Such structures can be useful for catalytic purposes and are concurrent with other studies (Figueiredo & Pereira, 2006). Of interest are the uniform macro-pores seen at the 50,000x magnification in Fig. 3c and d.

Further analysis of the surface microstructure was obtained with TEM imaging. Similar to other carbon surfaces with a high surface area, a worm-like uniform surface is observed (Ashourirad et al., 2015; Luo et al., 2014). Similar fringe images of graphitizable and non-graphitizable carbon have been published by Marsh and Rodriguez-Reinoso (2006). The parallelism of the carbon layers observed in Fig. 4 show a top down view of the sheets of cellulose, the material used to develop this nitrogen doped char.

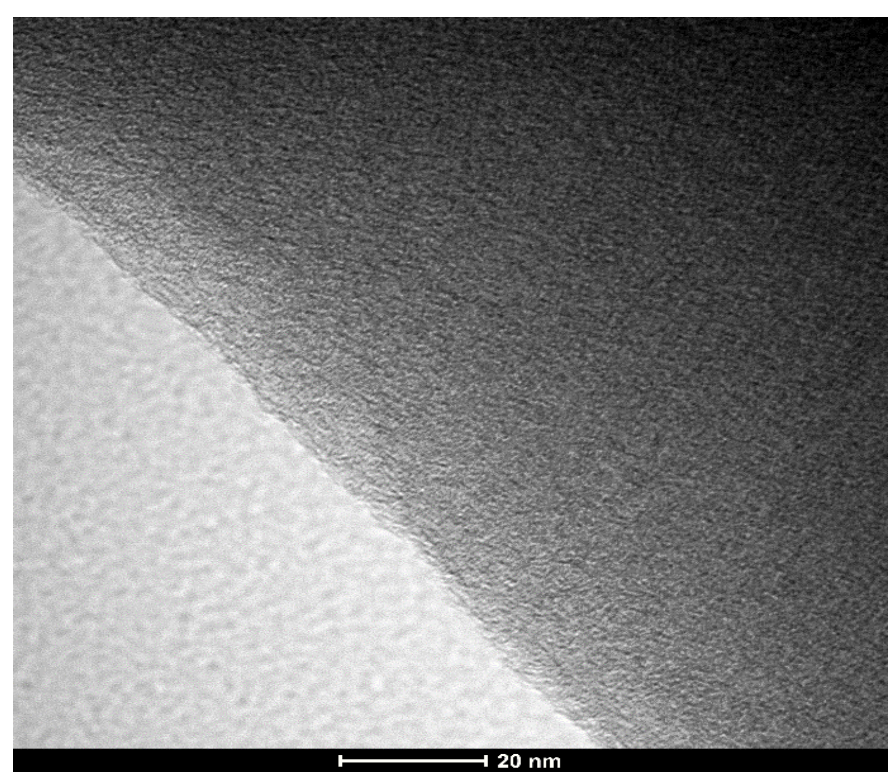
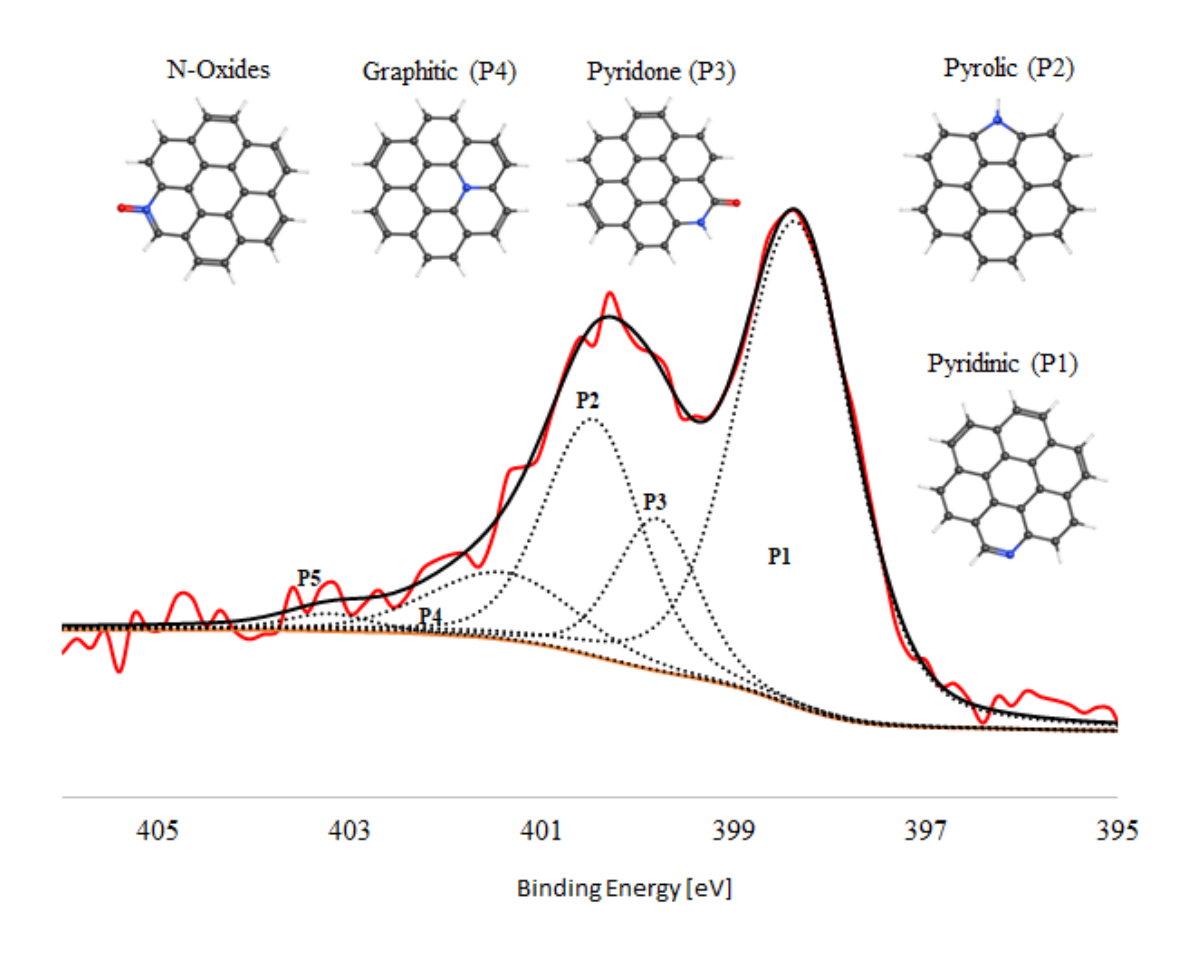


**Figure 4.** TEM images of nitrogen doped cellulose char surface displaying a worm like uniform pattern.

#### 3.2. XPS analysis

In order to advance understanding of the functionalized surface of the N-doped char catalysts, X-ray photon spectroscopy was conducted for all the samples produced. Figure 5 shows the N1s XPS spectra specifically for the N-doped char sample produced at 850 °C

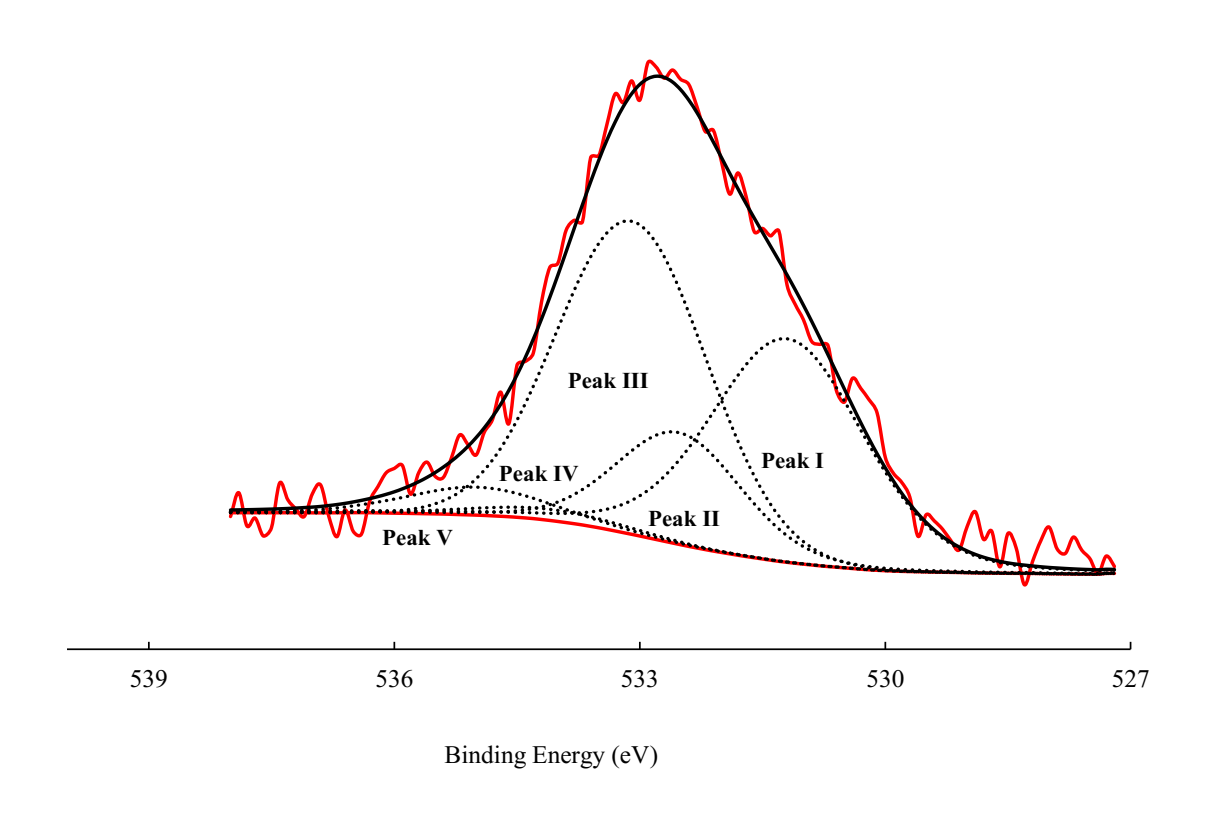
due to its high surface area and best candidacy as a catalyst. The subsequent deconvolution was conducted to identify the major types of N-groups present in this sample. In total, six nitrogen groups were identified and quantified: Pyridinic (P1): 54.1 atom%; Pyrolic (P2): 22.5 atom%; Pyridone (P3): 12.4 atom%; Graphitic (P4): 9.0 atom%; and N-oxides (P5): 1.3 atom%. The pyridinic N is also known as the N-6 group due to a single nitrogen replacing a carbon in a 6-membered ring. The Pyridinic group has been reported in the literature as having a favorable impact on wet oxidation applications (Soares et al., 2016).



**Figure 5.** N-1s XPS peak deconvolution of pyridinic (P1), pyrolytic (P2), pyridine (P3), graphitic (P4) nitrogen groups, as well as N-oxides (P5). The grey, white, blue, and red spheres are C, H, N and O atoms, respectively.

As previously mentioned, a series of N-doped chars were developed under various temperature conditions. It was decided that due to the surface area increase at the highest temperature all kinetic tests would be conducted by N-doped char produced at 850 °C. Further XPS analysis was conducted to better understand the oxygenated functional groups

present on the surface of the N-doped char produced at 850 °C. The O1s XPS spectra seen in Fig. 6 shows that the largest percentage of oxygen was present in aromatic ether groups (Peak III). This is followed by a significant carbonyl functional group concentration as presented by Peak I. The complete functional group breakdown is listed in Table 1.



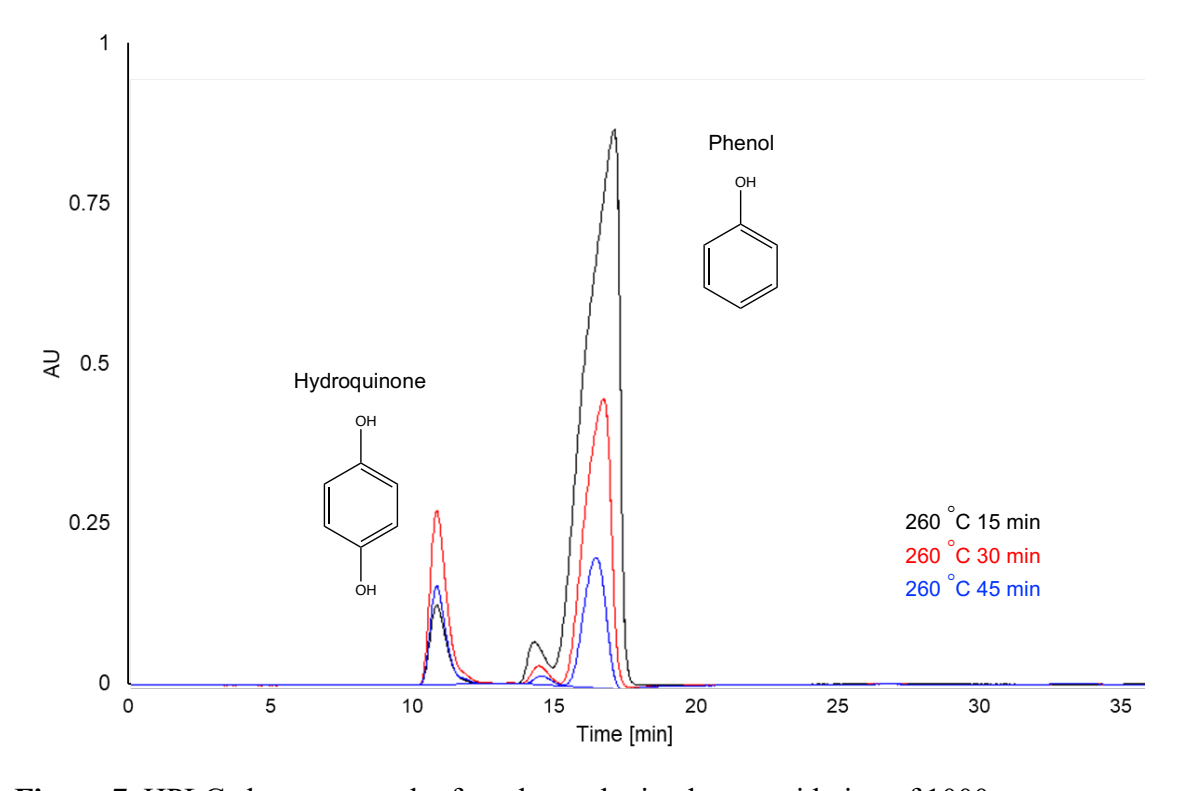
**Figure 6.** XPS peak deconvolution of O1s XPS spectrum. Functional groups represented in the char after deconvolution of carbonyl (Peak I), ether (aliphatic-peak II or aromatic-Peak III) and N-oxides (Peak IV). Peak V is due to moisture content (H<sub>2</sub>O).

Table 1. Quantified Oxygenated Groups in the N-doped Char Sample

Peak	Functional Groups	Oxygen Amount (%)
Peak I	C=O	33.5
Peak II	O-C (aliphatic)	2.50
Peak III	O-C (aromatic)	56.8
Peak IV	N=O	4.55
Peak V	Water	2.81

#### 3.3. Baseline oxidation tests

To develop a reproducible baseline to evaluate the catalytic effect of the N-doped chars, three preliminary tests were conducted without catalysts. HPLC analysis was used for quantification of phenol and primary byproducts such as hydroquinone. Figure 7 shows the chromatographs for 1000 ppm phenol decomposition at 15, 30 and 45 min under 260  $^{\circ}$ C and 1 MPa  $O_2$  partial pressure.



**Figure 7.** HPLC chromatograph of products obtained post oxidation of 1000 ppm aqueous phenol samples treated at 260 °C and 15, 30, and 45 min reaction time.

#### 3.4. Oxidation Reactor Tests without catalysts

This group of experiments was conducted with oxygen, but half of the tests the liquid was in contact with the stainless-steel tube, while in the other half were conducted within an inert glass liner. These experiments allowed us to study phenol oxidative reactions in the presence and absence of iron, a well-known oxidation catalyst. The result of these preliminary experiments is shown in Fig. 8a. The addition of O<sub>2</sub> definitively accelerates phenol oxidation. The most extreme reduction occurs at the higher temperature and reaction time conditions as seen in Fig. 8. A combination of temperature and time durations were tested in these initial experiments and it was concluded that operation above 260 °C and up to 45 min of reaction time, in the presence of oxygen, did not yield significantly improved results. This is likely due to a greater formation of free hydroxyl radicals at such conditions. Although the results are consistent with published data (Levec, Janez; Pintar, 1992) there exists little to no discussion of the effect of oxygen on stainless steel walls of such batch reactors. When compared with the results in the glass lined reactors, it is clear that the stainless reactors accelerated the oxidation of phenol considerably.

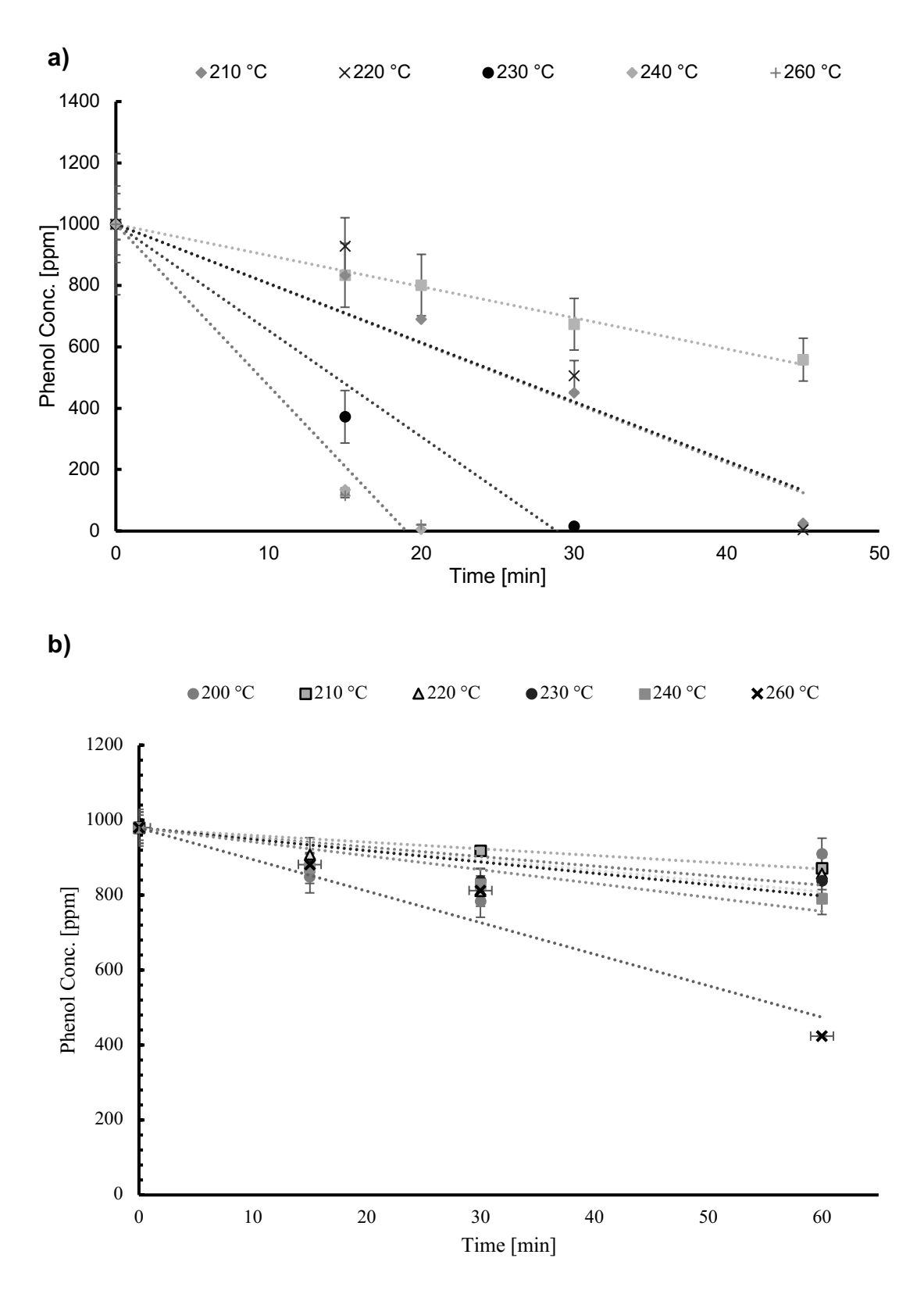


**Figure 8**. Result of reaction experiments a) under oxygen in a stainless-steel tube reactor and b) under oxygen, liquid in contact with glass. All experiments were conducted between 190 and 260 °C and at an oxygen partial pressure of 1 MPa.

Arrhenius parameters corresponding to each reaction setup (glass *vs.* stainless steel reactor wall) were calculated utilizing the integral method as discussed in the Materials and Method section. The Arrhenius plots for oxidation tests conducted with liquid in contact with stainless steel and glass are shown in Fig. 9. The activation energy obtained with the stainless-steel tube reactor was lower (67.5 kJ/mol) than the activation energy obtained for the glass tube (82.2 kJ/mol). However, the reaction rate constant was an order of magnitude higher. Most wet air oxidation studies and published reaction rate expressions have been catalogued for a wide range of operating conditions (Levec 1992; Migklez *et al.* 1997). Because of this, there is a large range of values for the activation energy data varying from 30 kJ/mol to 100 kJ/mol. The experimental values are clearly within the range reported in the literature (Levec 1992; Migklez *et al.* 1997).

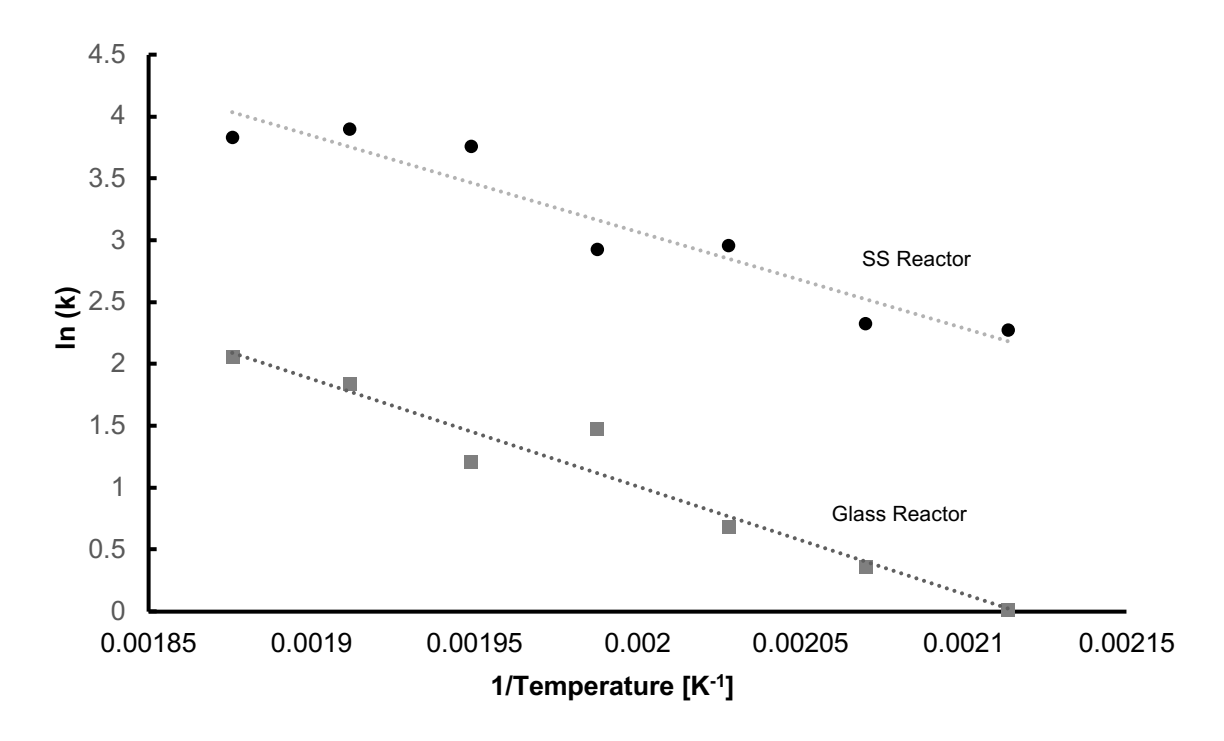


Figure 9. Arrhenius plot of phenol oxidation reaction with the SS and glass reactors.

Production of secondary products in the oxidation pathway of phenol is well known and understood (Devlin and Harris 1984; Bhargava *et al.* 2016). Hydroquinone can often be seen as the first product in the oxidation pathway. Hydroquinone was analyzed by HPLC and concentration change with respect to time and temperature can be seen in Figure 1SI. Specifically, hydroquinone will accumulate over the course of the 45 min reaction at low temperatures, indicating a slower oxidation. However, at higher temperatures and same reaction times lower concentrations of hydroquinone are found. Here oxidation is occurring

to a greater extent and intermediate products are being used up quickly.

### 3.5. Catalytic Oxidation Tests

Nitrogen doped chars, developed for this study and described above, introduced specific functional groups onto the surface of the catalyst, which had a significant effect on the catalytic wet oxidation of phenol. Initial screening conditions of 260 °C and 15, 30 and 45 min were chosen to ascertain if any catalytic properties existed. Figure 11 examines the catalytic capabilities of a non-doped char, a classical oxidation catalyst (CuSO<sub>4</sub>) and the N-doped char developed. All catalyst loading was set at 0.2 wt% with 1 MPa O<sub>2</sub> partial pressure. The catalyst loading was selected in order to find the minimum threshold for the CWO reaction to occur. The loading is significantly less than that of other heterogeneous catalysts reported and on the lower end for active carbon supported catalysts (Kolaczkowski, Plucinski, Beltran, Rivas, & McLurgh, 1999; Stüber et al., 2005). Results indicate that the N-doped char has a similar catalytic capability in oxidizing phenol as the CuSO<sub>4</sub> by the end of the 45 min reaction. CuSO<sub>4</sub> is more active at shorter time durations, which is beneficial in process design. However, well-documented issues of copper leaching are a challenge for this and other metal salt catalysts (Bhargava et al., 2006; Kolaczkowski et al., 1999). Their cost of production also makes them less desirable than a renewable, inexpensive, and environmentally sustainable catalysts such as N-doped char.

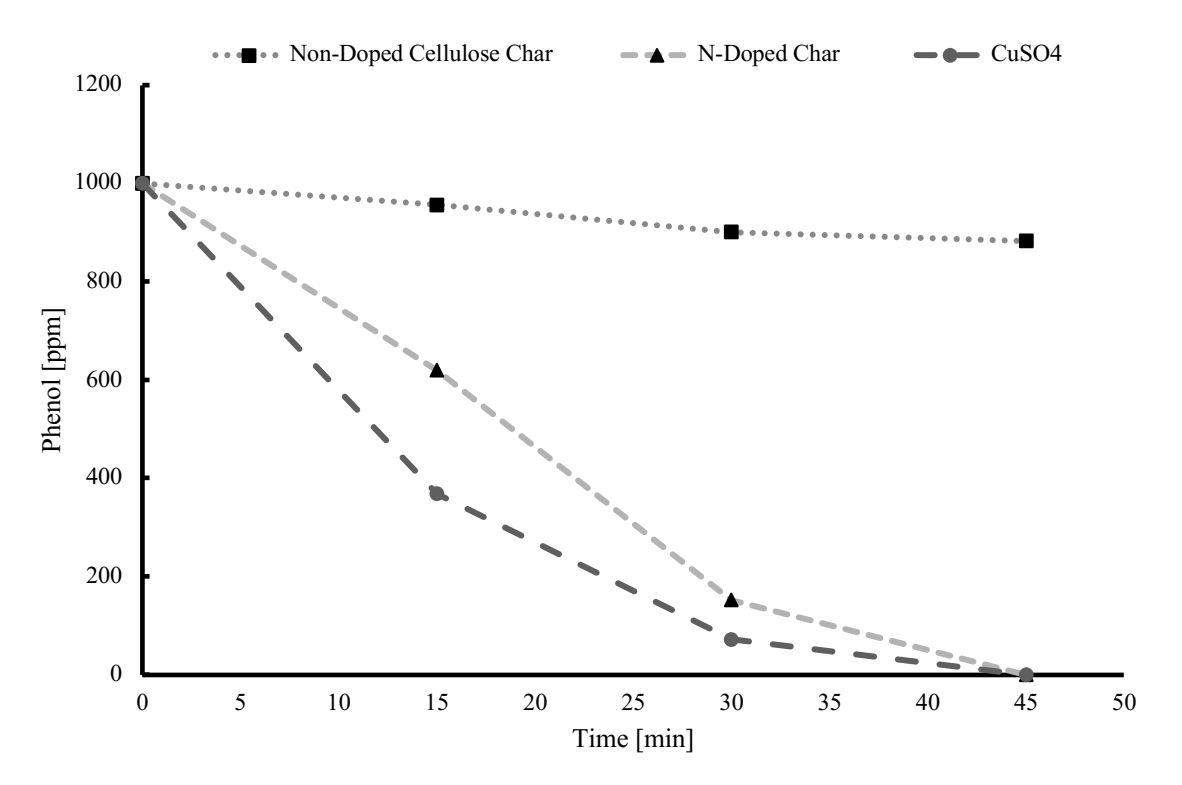


**Figure 11.** Initial screening of removal of phenol from an aqueous product by classic heterogeneous and novel N-doped oxidation catalysts.

Further evaluation of the impact of temperature on the catalytic oxidation using N-doped char was conducted based on the favorable initial results. Figure 12 shows the evolution of phenol concentration for an oxidation reaction conducted at a catalyst loading of 0.2 wt% in the glass reactor. The complete conversion of phenol is observed at both 250 °C and 260 °C at the 45 min residence time. These reactions follow the same pseudo first order kinetic rate observed in previous non-catalytic reactions.

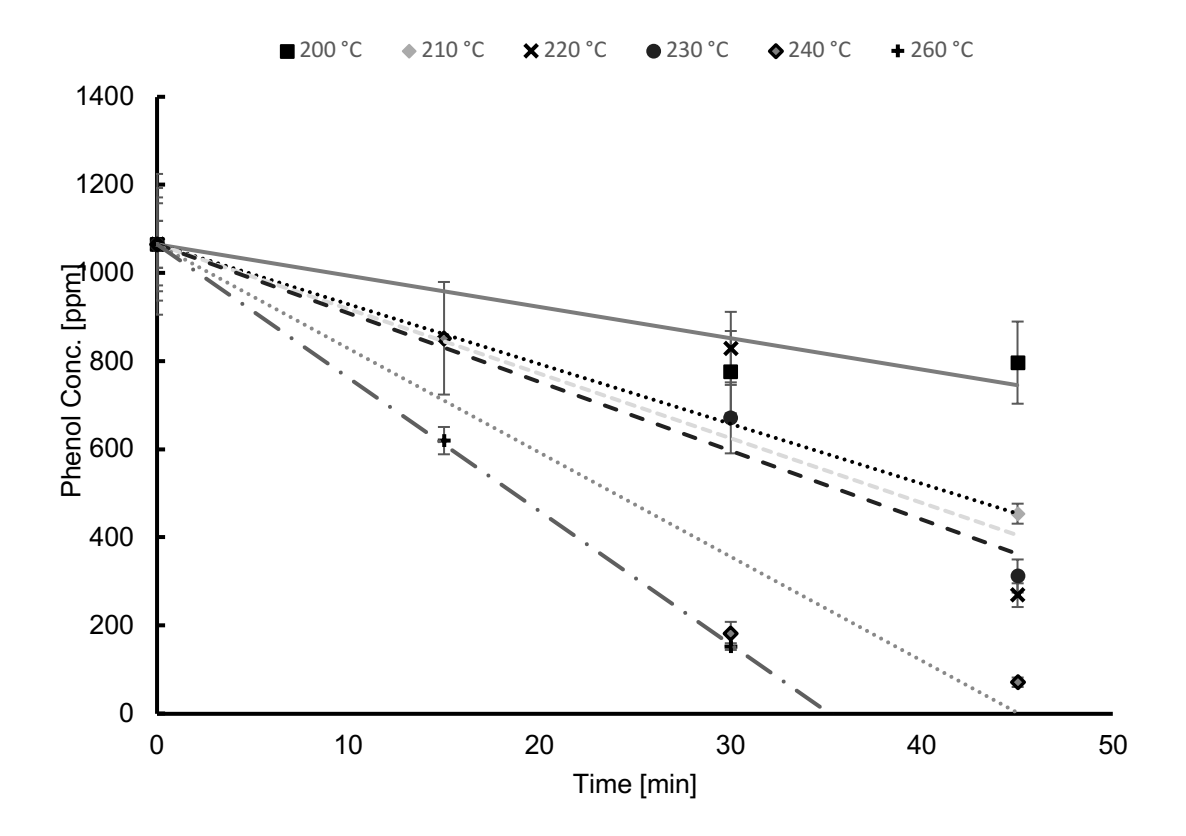


**Figure 12.** Phenol oxidation in presence of O<sub>2</sub> and nitrogen doped char catalyst in glass lined reactors. Catalyst loading at 0.2 wt. %

To gain more insight into the temperature impact on the CWO of phenol with N-doped catalyst, hydroquinone produced in the first oxidation step was tracked. Figure 2SI shows a lower concentration of hydroquinone at higher temperatures or longer reaction times. This result supports the data in Fig. 9 indicating complete phenol oxidation. However, the presence of such intermediates even at the most extreme conditions indicates that complete carbonization of all organic products to CO<sub>2</sub> and H<sub>2</sub>O (as proposed by Devlin and Harris (1984)) did not occur.

Figure 14 shows the Arrhenius plot of the reaction rate constant for oxidation reactions in the presence of N-doped chars. The use of this catalyst reduced the activation energy from 72 kJ/mol to 40 kJ/mol and increased the reaction rate constant by an order of magnitude compared with the tests without catalysts.

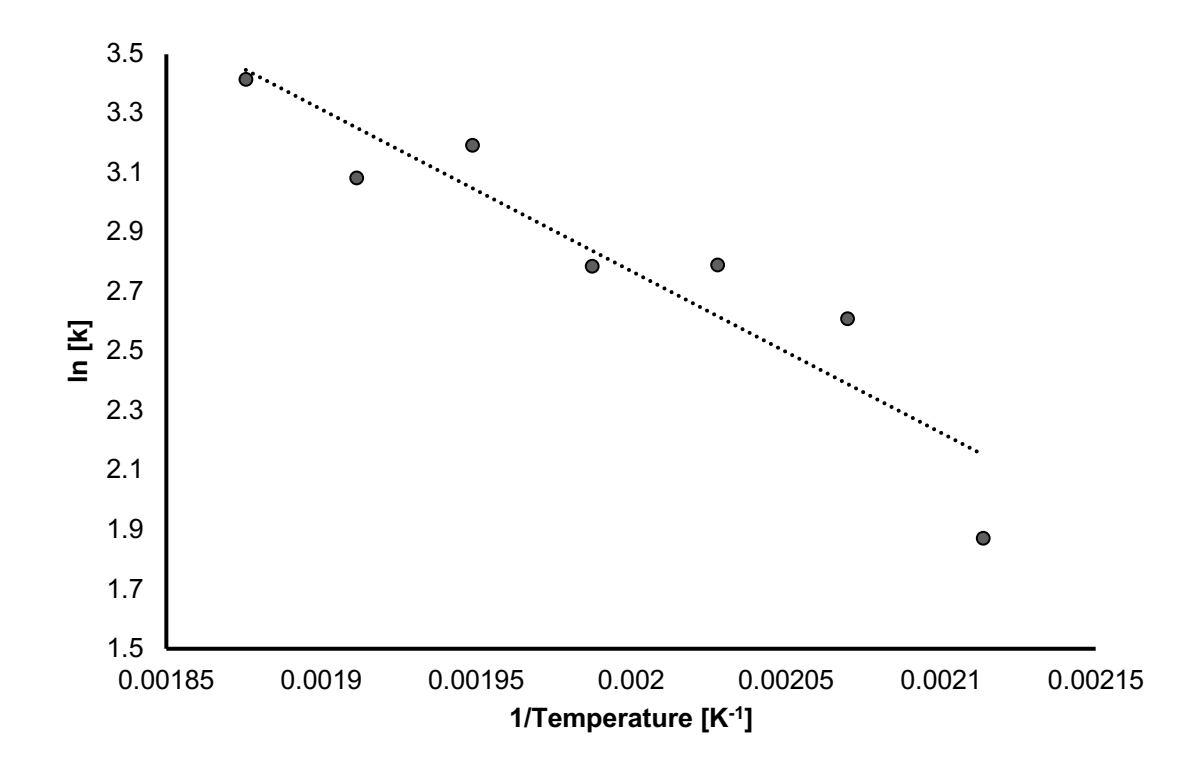


**Figure 14.** Energy of activation for nitrogen doped char catalyzed phenol oxidation reactions.

Introducing nitrogen functionalities in char structures, as a form of functionalization of a carbon surface, has been studied for several decades (Kapteijn, Moulijn, Matzner, & Boehm, 1999; Luo et al., 2014; Mood, Ayiania, Jefferson-Milan, & Garcia-Perez, 2020) The production mechanism is also well understood (Rocha et al., 2017). However, the exact functional group(s) responsible for the most significant oxidative catalytic effect observed is in the early stages of exploration often informed through novel techniques such as XPS and DFT analysis. Our team produced N-doped chars from cellulose at 400 °C, 500 °C, 600 °C, and 700 °C based on previously published methods (Smith et al., 2016). Detailed XPS analysis of each char's surface functional groups were conducted, and the functional groups of these chars reported (Ayiania et al., 2020). In the preliminary wet oxidation studies reported here, all chars were used as catalysts in addition to one produced at 850 °C. Catalytic wet oxidation of phenol at 240 °C, 2 MPa partial O<sub>2</sub> pressure, and a reaction time of 45 min was conducted using the five catalysts. Ayiania (Ayiania et al.,

2020) used XPS analysis, as reproted here, to identify the composition of nitrogen functional groups. Coupled with the characterization conducted in the 850 °C char catalyst a range of pyridinic functional groups were identified. As seen in Figure 15 an experimental correlation between increasing pyridinic group content of char, and the reduction in final phenol concentration, was observed. This result would suggest that there is a correlation between the pyridinic functional group, and the oxidative catalytic effect observed.

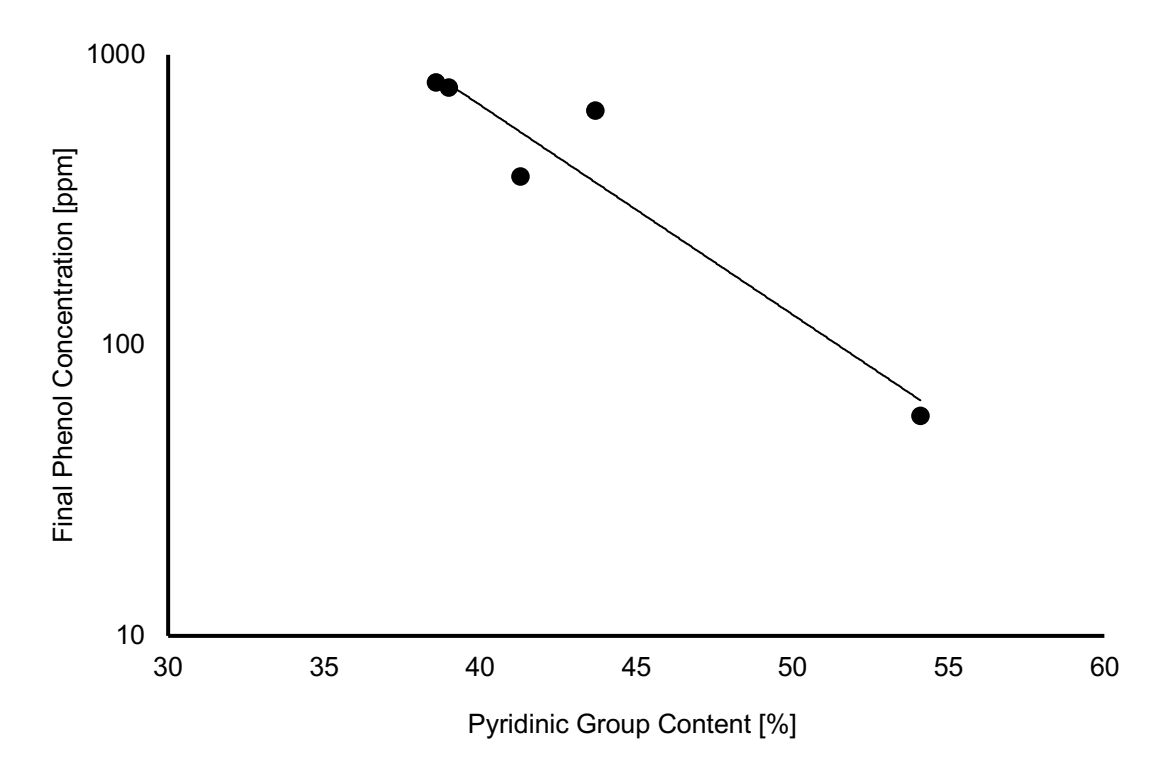


**Figure 15.** Preliminary results on the effect of phenol reduction in the presence of increasing pyridinic groups present on the char surface.

#### 3.6.DFT Analysis

A density functional theory analysis was used to ascertain the specific functionalities responsible for the possible catalytic activity of the nitrogen-doped char. As the formation of reactive oxygen species is the rate-limiting step for the reaction at hand, (Kolaczkowski et al., 2002; Rivas et al., 1998) sites were tested for their ability to do so from both water and oxygen. In general, water was found to be inert with respect to all active sites tested, while as expected oxygen showed significant activity. Water only chemisorbed to the 4N6 site while favorably hydrogen bonding to almost all others, which is consistent with its high stability. Because the reaction energies calculated are relative to gas-phase water, their

adsorption strength is a meaningful test of relative reactivity between sites, rather than an absolute energy change at reaction conditions. We find that the dipole moment of water interacts effectively with charge differentials created by defects and heteroatomic dopants, but that the reaction energies are low. Oxygen, on the other hand, chemisorbs to multiple sites.

To establish a computational baseline for char without surface modifications, chemically homogenous carbon models (perfect graphene and a 585 defect) were tested for reactivity with both water and oxygen. The structures for these models are discussed in the supplementary information. The 585 defect, consisting of a graphene divacancy reformed into two pentagons and an octagon, is shown in Figure 16 as a litmus test for carbon activity. While results were consistent for both carbon sites, this functionality was deemed the best potential indicator due to its high reactivity and documented occurrence (Denis & Iribarne, 2013). As shown in Table 1 and Figure 16, the site favorably adsorbs a water molecule onto its surface and is aggressively oxidized by diatomic oxygen with binding energies of -622 kJ/mol.

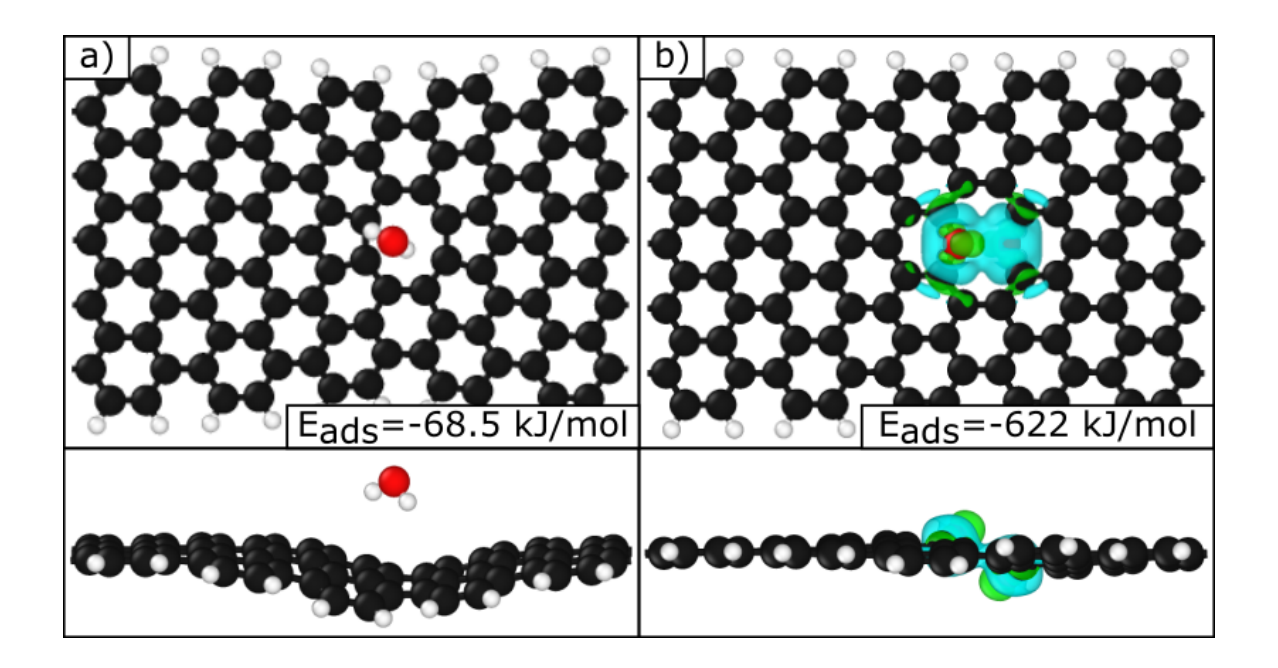


**Figure 16.** A differential charge analysis of (a) water (a) and (b) oxygen adsorbed to a 585 divacancy within a graphene ribbon. White, black, and red indicate H, C, and O atoms, respectively. Blue indicates an increase in electron density relative to the isolated reactants, while green indicates the converse. The isosurface level shown is  $0.025 \ e/Bohr^3$ .

**Table 2.** Oxygen and Water Binding Energies of all Active Sites Tested.

Structure	Structure Class	O <sub>2</sub> Binding Energy (kJ/mol)	H <sub>2</sub> O Binding Energy (kJ/mol)
4N6 Defect	Pyridinic	34	-29
Di-pyrindinic Edge	Pyridinic	-20	-37
Pyridinic Edge	Pyridinic	80	-28
Pyrrolic Edge	Pyrrolic	22	-41
585 Defect	Graphene	-622	-69
Graphene	Graphene	48	-9.4
Graphene Hydrogen Divacancy	Graphene	-540	N/A
Graphitic Edge	Graphitic	42	-8.3
Graphitic Sheet	Graphitic	-15	-6.7

As can be seen by examining Table 2, we show that all un-doped carbon sites are likely to be inert with respect to the solvent or will form oxides irreversibly in the presence of oxygen. In an experimental context, this indicates that the sites are unlikely to produce any sort of active oxygen species, either from the solvent or any oxygen present in solution. While N defects were similarly inert in the presence of water, they displayed a mixed reactivity to oxygen. Almost all were found to induce barrierless splitting of oxygen molecules brought nearby, although most resulted in an unfavorable, metastable chemisorption of the split molecule. The 4N6 active site was found to favorably split water, due to its unique sterics and availability of four pyridinic nitrogen atoms within the plane of the graphene sheet. However, these reactive divacancies have a very high formation energy, and are extremely rare under the experimental conditions of the present work (Ayiania, Hensley, et al., 2019). In general, N sites hydrogen-bonded to water and formed unfavorable oxide species on the edge of the char, making them mediocre candidates for oxygen activation.

The most promising catalytic results with the N-doped char were found with the dipyridinic site shown in Figure 17. XPS and thermodynamic data indicate these functionalities to be extremely common in N-doped char, and very stable when formed as an edge site (Ayiania, Hensley, et al., 2019). Of all sites tested, these alone favorably split and bound oxygen molecules. In addition, their low binding energy (-0.2 eV) makes their adsorption reversible, allowing them to maintain catalytic activity. Coupled with the XPS analysis presented above, the dipyridinic group is the most likely active site for catalytic oxidation

reactions under the conditions studied.

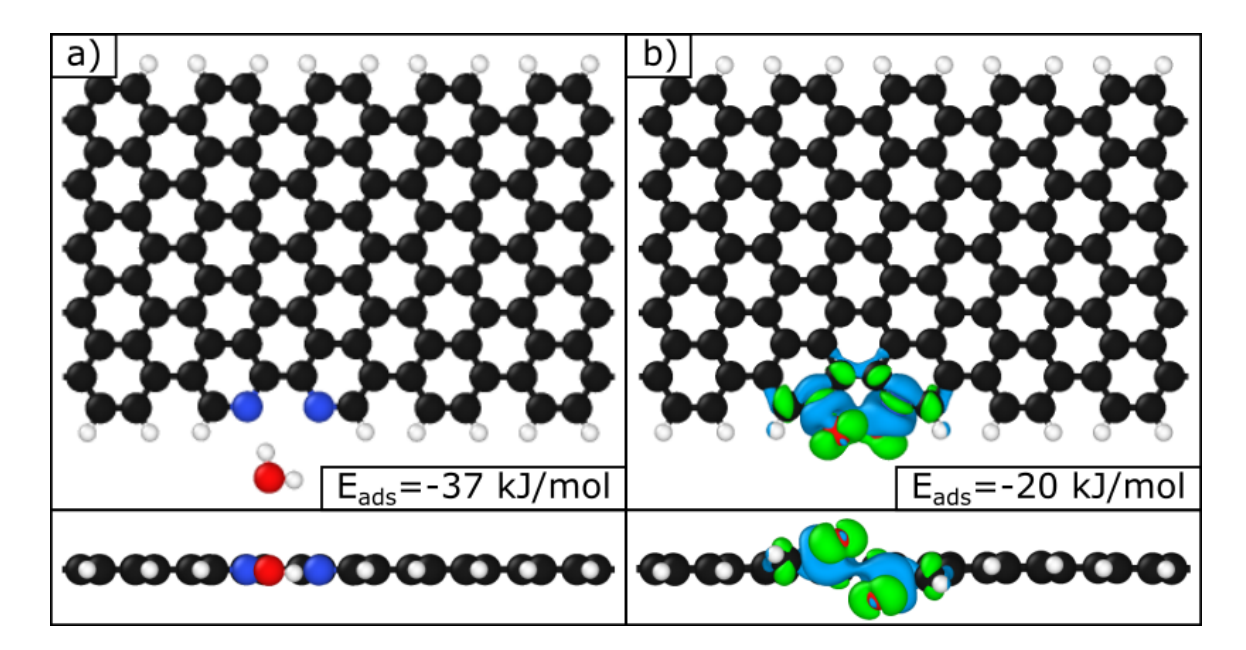


**Figure 17.** A differential charge diagram of water (a) and oxygen (b) adsorbed to a dipyridinic site on the edge of a graphene ribbon. White, black, and red indicate H, C, and O atoms, respectively. Blue indicates an increase in electron density relative to the isolated reactants, while green indicates the converse. The isosurface level shown is 0.025  $e/Bohr^3$ .

#### 3.7 Overview of results

The overall consumption of the phenol during the reaction in our tube reactor (see Figure 3SI), can be attributed to a number of physico-chemical phenomena. The first step consists on the solubilization of  $O_2$  and its diffusion to the surface of the catalyst. The saturation (solubilization of  $O_2$ ) in the aqueous phase depends on the partial pressure of the  $O_2$  in gas phase. The diffusion is typically controlled by the level of mixing and turbulence in the reactor.

Two events on the surface are thought to be increasing the concentration of free radicals (mainly OH·) in the system. First, the addition of nitrogen functional groups on the surface of the char catalyst is known to produce basic surfaces which can drive electron transfer (Figueiredo & Pereira, 2006). As seen from the deconvolution of the XPS data the N-doped char catalyst contains a high concentration of pyridinic groups. Our DFT analysis confirms the hypothesis that a pyridinic group could be responsible for propagation of hydroxy free

radicals. Specifically, the dipyridinic group was found to be the most energetically favorable in binding and splitting O<sub>2</sub>. This creates a suitable environment for hydroxyl free radical formation, which is key to the phenol oxidation mechanism.

#### 4. Conclusions

Developing an alternative catalyst for catalytic wet oxidation of phenol can be accomplished through the production of N-doped chars. Using ammonia exposure methods at 850 °C, N-functionalities were incorporated into cellulose char. Much of the nitrogen was concentrated in pyridinic functionalities introduced onto the char surface. Reaction rate kinetic parameters for each experimental setup were developed for comparison and the results indicated a decrease in the activation energy of CWAO reactions with N-doped char. This is due to the increase of free radical formation both in the aqueous phase as well as on the surface of the char due to the added basic nitrogen functional groups. Our DFT studies found the dipyridinic group to be the most energetically favorable in binding and splitting O<sub>2</sub>. This step is critical for the formation of free radicals. Future studies will include other dopants such as sulfur utilizing woody and agro biomasses in order to assess the efficacy of the oxidation contributed by other bio-polymers and the effect of ash.

Acknowledgements: The authors thank the Sun Grant subproject, Grant No. 128467-G004003. J.-S.M and A.G. were supported by the National Science Foundation under Contract No. CBET-1703052. Special thanks to Jonathan Lamber of WSU Analytical Chemistry Service Center for his assistance in support of this work, Yaime Jefferson for her analytical support, Katie Johnson of the NARA Summer Intern in the Garcia-Perez Laboratory, and Roberto Esquivel for the graphic support. This research used resources from the Center for Institutional Research Computing at Washington State University. This work was partially funded by the Joint Center for Deployment and Research in Earth Abundant Materials (JCDREAM) in Washington State. PNNL is a multiprogram national laboratory operated for the US DOE by Battelle.

#### **References:**

Adib, F., Bagreev, A., and Bandosz, T. J. (2000). "Adsorption/oxidation of hydrogen sulfide on nitrogen-containing activated carbons," *Langmuir* 16(4), 1980-1986. DOI: 10.1021/la9909260

- Agency for Toxic Substances and Disease Registry (ATSDR) (2018). "Toxicological profile: Phenol," (https://www.atsdr.cdc.gov/toxprofiles/tp.asp?id=148&tid=27>), Accessed 26, February 2019.
- Alnaizy, R., and Akgerman, A. (2000). "Advanced oxidation of phenolic compounds," *Advances in Environmental Research* 4(3), 233-244. DOI: 10.1016/S1093-0191(00)00024-1
- Arena, F., Negro, J., Parmaliana, A., Spadaro, L., and Trunfio, G. (2007). "Improved MnCeO<sub>x</sub> systems for the catalytic wet oxidation (CWO) of phenol in wastewater streams," *Industrial and Engineering Chemistry Research* 46(21), 6724-6731. DOI: 10.1021/ie0701118
- Ashourirad, B., Sekizkardes, A. K., Altarawneh, S., and El-Kaderi, H. M. (2015). "Exceptional gas adsorption properties by nitrogen-doped porous carbons derived from benzimidazole-linked polymers," *Chemistry of Materials* 27(4), 1349-1358. DOI: 10.1021/cm504435m
- Ayiania, M., Carbajal-Gamarra, F. M., Garcia-Perez, T., Frear, C., Suliman, W., and Garcia-Perez, M. (2019). "Production and characterization of H<sub>2</sub>S and PO<sub>4</sub><sup>3-</sup> carbonaceous adsorbents from anaerobic digested fibers," *Biomass and Bioenergy* 120, 339-349. DOI: 10.1016/J.BIOMBIOE.2018.11.028
- Ayiania, M., Smith, M., Hensley, A. J. R., Scudiero, L., McEwen, J. S., & Garcia-Perez, M. (2020). "Deconvoluting the XPS spectra for nitrogen-doped chars: An analysis from first principles," *Carbon* 162, 528–544. https://doi.org/10.1016/j.carbon.2020.02.065
- Bhargava, S. K., Tardio, J., Prasad, J., Fo, K., Akolekar, D. B., and Grocott, S. C. (2006). "Wet oxidation and catalytic wet oxidation," *Industrial and Engineering Chemistry Research*, 45(4), 1221-1258. DOI: 10.1021/ie051059n
- Blume, R., Rosenthal, D., Tessonnier, J.-P., Li, H., Knop-Gericke, A., and Schlögl, R. (2015). "Characterizing graphitic carbon with X-ray photoelectron spectroscopy: A step-by-step approach," *ChemCatChem* 7(18), 2871-2881. DOI: 10.1002/cctc.201500344
- Chen, H., Sun, F., Wang, J., Li, W., Qiao, W., Ling, L., and Long, D. (2013). "Nitrogen doping effects on the physical and chemical properties of mesoporous carbons," *Journal of Physical Chemistry C* 117(16), 8318-8328. DOI: 10.1021/jp4017773
- Devlin, H. R., and Harris, I. J. (1984). "Mechanism of the oxidation of aqueous phenol with dissolved oxygen," *Industrial and Engineering Chemistry Fundamentals* 23(4),

- 387-392. DOI: 10.1021/i100016a002
- Ding, D., Yang, S., Qian, X., Chen, L., Cai, T. "Nitrogen-doping positively whilst sulfur-doping negatively affect the catalytic activity of biochar for the degradation of organic contaminant." *Applied Catalysis B: Environmental* 263(1): 118348. DOI: 10.1016/j.apcatb.2019.118348
- Duan W, Meng F, Cui H, Lin Y, Wang G, Wu J (2018) "Ecotoxicity of phenol and cresols to aquatic organisms: A review". *Ecotoxicology and Environmental Safety*. Volume 157, 2018, 441-456
- Eisenhauer, H. R. (1964). "Oxidation of phenolic wastes," *Water Pollution Control Federation* 36(9), 1116-1128. DOI: 10.1177/03063127067078012
- Eisenhauer, H. R. (1971). "Increased rate and efficiency of phenolic waste ozonization," *Water Pollution Control Federation* 43(2) 200-208.
- Estrade-Szwarckopf, H. (2004). "XPS photoemission in carbonaceous materials: A 'defect' peak beside the graphitic asymmetric peak," *Carbon* 42(8-9), 1713-1721. DOI: 10.1016/J.CARBON.2004.03.005
- Fang, G., Gao, J., Liu, C., Dionysiou, D. D., Wang, Y., and Zhou, D. (2014). "Key role of persistent free radicals in hydrogen peroxide activation by biochar: Implications to organic contaminant degradation," *Environmental Science and Technology* 48(3), 1902-1910. DOI: 10.1021/es4048126
- Fang, G., Liu, C., Gao, J., Dionysiou, D. D., and Zhou, D. (2015). "Manipulation of persistent free radicals in biochar to activate persulfate for contaminant degradation," *Environmental Science and Technology* 49(9), 5645-5653. DOI: 10.1021/es5061512
- Figueiredo, J. L., and Pereira, M. F. R. (2006). "Carbon as catalyst," in: *Carbon Materials for Catalysis*, John Wiley & Sons Inc., Hoboken, New Jersey, USA, pp. 177-217.
- He, S., Bijl, A., Barana, P. K., Lefferts, L., Kersten, S. R. A., & Brem, G. (2020). "Recycling Strategy for Bioaqueous Phase via Catalytic Wet Air Oxidation to Biobased Acetic Acid Solution," *ACS Sustainable Chemistry & Engineering* 8(39), 14694–14699. DOI:10.1021/acssuschemeng.0c05946
- Imamura, S. (1999). "Catalytic and noncatalytic wet oxidation," *Industrial and Engineering Chemistry Research* 38(5), 1743-1753. DOI: 10.1021/ie9805761
- Javier Benitez, F., Acero, J. L., Gonzalez, T., and Garcia, J. (2001). "Organic matter removal from wastewaters of the black olive industry by chemical and biological procedures," *Process Biochemistry* 37(3), 257-265. DOI: 10.1016/S0032-

- 9592(01)00209-6
- Klüpfel, L., Keiluweit, M., Kleber, M., and Sander, M. (2014). "Redox properties of plant biomass-derived black carbon (biochar)," *Environmental Science and Technology* 48(10), 5601-5611. DOI: 10.1021/es500906d
- Kolaczkowski, S. T., Beltran, F. J., McLurgh, D. B., and Rivas, F. J. (2002). "Wet air oxidation of phenol," *Process Safety and Environmental Protection* 75(4), 257-265. DOI: 10.1205/095758297529138
- Kolaczkowski, S. T., Plucinski, P., Beltran, F. J., Rivas, F. J., and McLurgh, D. B. (1999)."Wet air oxidation: A review of process technologies and aspects in reactor design,"Chemical Engineering Journal 73(2), 143-160. DOI: 10.1016/S1385-8947(99)00022-4
- Krasheninnikov, A. V, and Nieminen, R. M. (2011). "Attractive interaction between transition-metal atom impurities and vacancies in graphene: A first-principles study," *Theoretical Chemistry Accounts* 129(3-5), 625-630. DOI: 10.1007/s00214-011-0910-3
- Kulkarni SJ, Kaware JP (2013) "Review on Research for Removal of Phenol from Wastewater", International Journal of Scientific and Research Publications, Volume 3, 4, 1-5
- Lee, D. H., Lee, W. J., Lee, W. J., Kim, S. O., and Kim, Y.-H. (2011). "Theory, synthesis, and oxygen reduction catalysis of Fe-porphyrin-like carbon nanotube," *Physical Review Letters* 106(17), 175502. DOI: 10.1103/PhysRevLett.106.175502
- Lefèvre, M., Proietti, E., Jaouen, F., and Dodelet, J.-P. (2009). "Iron-based catalysts with improved oxygen reduction activity in polymer electrolyte," *Science* 324(5923), 71-74. DOI: 10.1126/science.1170336
- Levec, J. (1992). "Catalytic oxidation of toxic organics in aqueous solution," *Applied Catalysis* 63, 345-357. DOI: 10.1016/S0166-9834(00)81700-5
- Liotta, L. F., Gruttadauria, M., Di Carlo, G., Perrini, G., & Librando, V. (2009). "Heterogeneous catalytic degradation of phenolic substrates: Catalysts activity," *Journal of Hazardous Materials*. https://doi.org/10.1016/j.jhazmat.2008.05.115
- Liu, C., Chen, L., Ding, D., & Cai, T. (2019). "From rice straw to magnetically recoverable nitrogen doped biochar: Efficient activation of peroxymonosulfate for the degradation of metolachlor." *Applied Catalysis B: Environmental*, 254, 312–320. DOI: 10.1016/j.apcatb.2019.05.014

- Lomnicki, S., Truong, H., Vejerano, E., and Dellinger, B. (2008). "Copper oxide-based model of persistent free radical formation on combustion-derived particulate matter," *Environmental Science and Technology* 42(13), 4982-4988. DOI: 10.1021/es071708h
- Luo, W., Wang, B., Heron, C. G., Allen, M. J., Morre, J., Maier, C. S., Stickle, W. F., and Ji, X. (2014). "Pyrolysis of cellulose under ammonia leads to nitrogen-doped nanoporous carbon generated through methane formation," *Nano Letters* 14(4), 2225-2229. DOI: 10.1021/nl500859p
- Marsh, H., and Rodriguez-Reinoso, F. (2006). Activated Carbon, Elsevier, London, UK.
- Miguelez, J. R. P., Bernal, J. L., Sanz, E. N., and de la Ossa, E. M. (1997). "Kinetics of wet air oxidation of phenol," *Chemical Engineering Journal* 67, 115-121.
- Muley, P. D., Henkel, C., Abdollahi, K. K., Marculescu, C., & Boldor, D. (2016). "A critical comparison of pyrolysis of cellulose, lignin, and pine sawdust using an induction heating reactor," Energy Conversion and Management, 117, 273–280
- Nandi, M., Okada, K., Dutta, A., Bhaumik, A., Maruyama, J., Derks, D., and Uyama, H. (2012). "Unprecedented CO<sub>2</sub> uptake over highly porous N-doped activated carbon monoliths prepared by physical activation," *Chemical Communications* 48(83), 10283-10285. DOI: 10.1039/c2cc35334b
- Pruden, B. B., and Le, H. (1976). "Wet air oxidation of soluble components in waste water," *Canadian Journal of Chemical Engineering* 54(4), 319-325.
- Rivas, F. J., Kolaczkowski, S. T., Beltran, F. J., and McLurgh, D. B. (1999). "Hydrogen peroxide promoted wet air oxidation of phenol: Influence of operating conditions and homogeneous metal catalysts," *Journal of Chemical Technology and Biotechnology* 74(5), 390-398. DOI: 10.1002/(SICI)1097-4660(199905)74:5<390::AID-JCTB64>3.0.CO;2-G
- Rivas, F. J., Kolaczkowski, S. T., Beltrán, F. J., and McLurgh, D. B. (1998). "Development of a model for the wet air oxidation of phenol based on a free radical mechanism," *Chemical Engineering Science* 53(14), 2575-2586. DOI: 10.1016/S0009-2509(98)00060-8
- Rocha, R. P., G.P. Soares, O. S., Gonçalves, A. G., Órfão, J. J. M., Pereira, M. F. R., & Figueiredo, J. L. (2017). "Different methodologies for synthesis of nitrogen doped carbon nanotubes and their use in catalytic wet air oxidation," *Applied Catalysis A: General* 548, 62–70. https://doi.org/10.1016/j.apcata.2017.08.033
- Rodríguez-Ramos, I., Oliviero, L., Bachiller-Baeza, B., Duprez, D., Barbier, J., and

- Guerrero-Ruiz, A. (2002). "Catalytic wet air oxidation of phenol and acrylic acid over Ru/C and Ru-CeO<sub>2</sub>/C catalysts," *Applied Catalysis B: Environmental* 25(4), 267-275. DOI: 10.1016/s0926-3373(99)00141-1
- Smith, M., Scudiero, L., Espinal, J., McEwen, J. S., & Garcia-Perez, M. (2016). Improving the deconvolution and interpretation of XPS spectra from chars by ab initio calculations," *Carbon* 110, 155–171. https://doi.org/10.1016/j.carbon.2016.09.012
- Soares, O. S. G. P., Rocha, R. P., Gonçalves, A. G., Figueiredo, J. L., Órfão, J. J. M., and Pereira, M. F. R. (2016). "Highly active N-doped carbon nanotubes prepared by an easy ball milling method for advanced oxidation processes," *Applied Catalysis B: Environmental* 192, 296-303. DOI: 10.1016/j.apcatb.2016.03.069
- Sun, F., Gao, J., Yang, Y., Zhu, Y., Wang, L., Pi, X., Liu, X., Qu, Z., Wu, S., and Qin, Y. (2016). "One-step ammonia activation of Zhundong coal generating nitrogen-doped microporous carbon for gas adsorption and energy storage," *Carbon* 109, 747-754. DOI: 10.1016/j.carbon.2016.08.076
- Sushma, K. M., and Saroha, A. K. (2018). "Performance of various catalysts on treatment of refractory pollutants in industrial wastewater by catalytic wet air oxidation: A review," *Journal of Environmental Management* 228(June), 169-188. DOI: 10.1016/j.jenvman.2018.09.003
- Tufano, V. (1993). "A multi-step kinetic model for phenol oxidation in high pressure water," *Chemical Engineering & Technology* 16(3), 186-190.
- Villegas, L. G. C., Mashhadi, N., Chen, M., Mukherjee, D., Taylor, K. E., and Biswas, N. (2016). "A short review of techniques for phenol removal from wastewater," *Current Pollution Reports* 2(3), 157-167. DOI: 10.1007/s40726-016-0035-3
- Wilson, A. N., Dutta, A., Black, B. A., Mukarakate, C., Magrini, K., Schaidle, J. A., Michener, W., Beckham, G., Nimlos, M. R. (2019). "Valorization of aqueous waste streams from thermochemical biorefineries," *Green Chemistry* 21(15), 4217–4230. DOI: 10.1039/c9gc00902g
- Wang, X., Li, X., Zhang, L., Yoon, Y., Weber, P. K., Wang, H., Guo, J., and Dai, H. (2009). "N-Doping of graphene through electrothermal reactions with ammonia," *Science* 324(5928), 768-771. DOI: 10.1126/science.1172260
- Wu, J. J., and Masten, S. J. (2002). "Oxidation kinetics of phenolic and indolic compounds by ozone: Applications to synthetic and real swine manure slurry," *Water Research* 36(6), 1513-1526. DOI: 10.1016/S0043-1354(01)00352-9

- Yang, J., Pan, B., Li, H., Liao, S., Zhang, D., Wu, M., and Xing, B. (2016). "Degradation of p-nitrophenol on biochars: Role of persistent free radicals," *Environmental Science and Technology* 50(2), 694-700. DOI: 10.1021/acs.est.5b04042
- Yao, Y., Gao, B., Chen, J., and Yang, L. (2013). "Engineered biochar reclaiming phosphate from aqueous solutions: Mechanisms and potential application as a slow-release fertilizer," *Environmental Science & Technology* 47(15), 8700-8708. DOI: 10.1021/es4012977
- Zhang, M., Gao, B., Varnoosfaderani, S., Hebard, A., Yao, Y., and Inyang, M. (2013). "Preparation and characterization of a novel magnetic biochar for arsenic removal," *Bioresource Technology* 130, 457-462. DOI: 10.1016/J.BIORTECH.2012.11.132

# **Supporting Information: Effect of Nitrogen Doped**

# **Char in Catalytic Wet Oxidation of Phenol**

## **Contaminated Water**

Iva Tews<sup>1</sup>, Aidan Garcia<sup>2</sup>, Michael Ayiania<sup>1</sup>, Sohrab Haghighi Mood<sup>1</sup>, Kalidas Mainali<sup>1</sup>, Jean-Sabin McEwen<sup>2, 3, 4, 5</sup> and Manuel Garcia-Perez<sup>1, 6</sup>

<sup>1</sup>Department of Biological Systems Engineering, Washington State University, Pullman, WA 99164, USA

<sup>2</sup>Gene and Linda Voiland School of Chemical Engineering and Bioengineering, Pullman, WA 99164, USA

<sup>3</sup>Department of Physics and Astronomy, Washington State University, Pullman, WA 99164
 <sup>4</sup>Department of Chemistry, Washington State University, Pullman, WA 99164
 <sup>5</sup>Institute for Integrated Catalysis, Pacific Northwest National Laboratory, Richland, WA, 99352
 <sup>6</sup>Bioproducts Science and Engineering Laboratory, Richland, WA 99354

Table S1: Adsorption Energies for All Sampled Reactive Sites				
Structure	O2 Adsorption Model	O2 Adsorption Energy (kJ/mol)	H20 Adsorption Model	H2O Adsorption Energy (kJ/mol)
4N6 Ribbon		34		-29
585		-622		-5.6

Di- pyrindinic	-20		-37
Graphene	48	<b>6</b> , 9000000000000000000000000000000000000	-9.4
Graphitic Edge	42		-8.3

Graphitic Sheet		
	-15	-6.7
Pyridinic	80	-28
Pyrrolic	22	-41

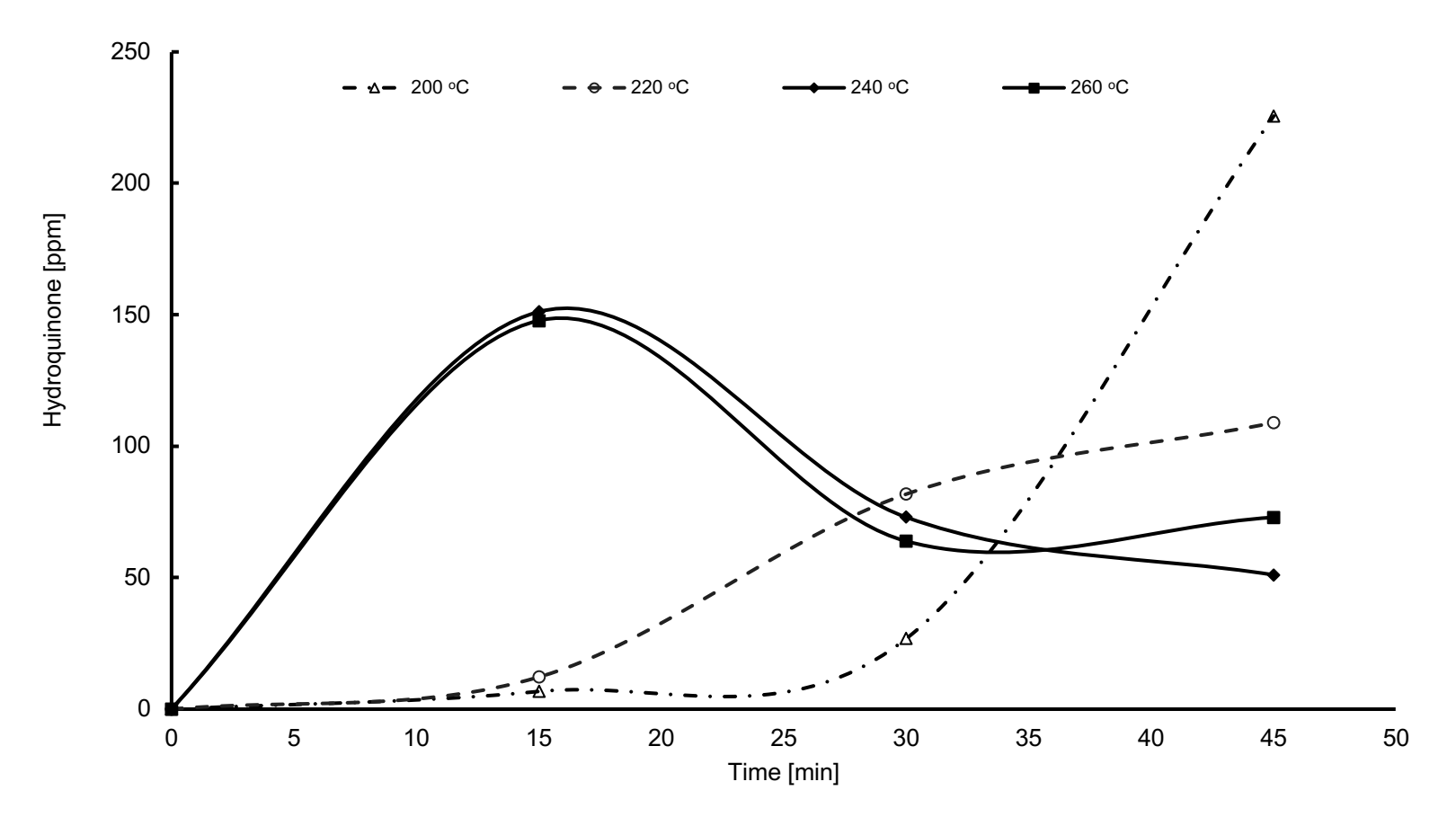
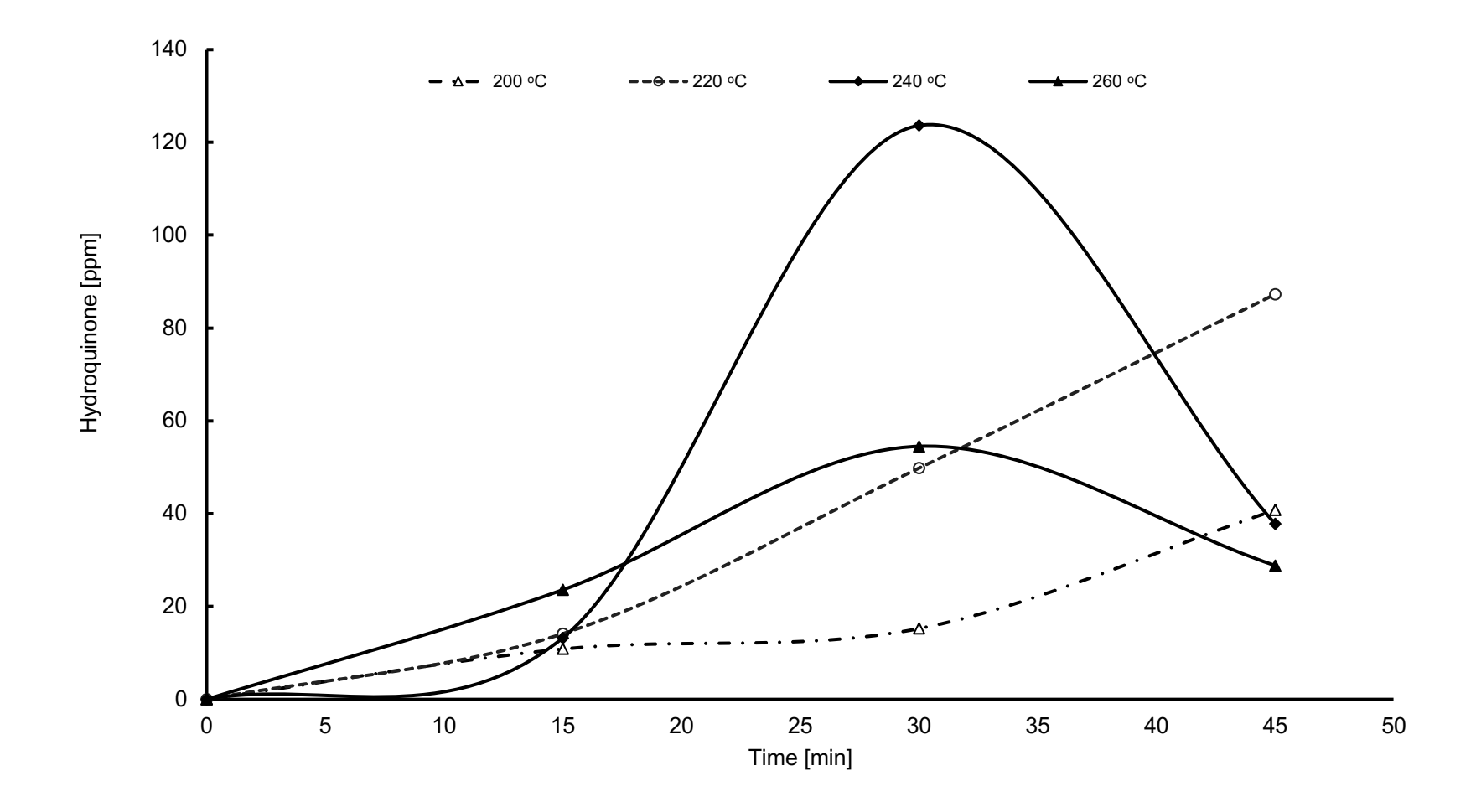
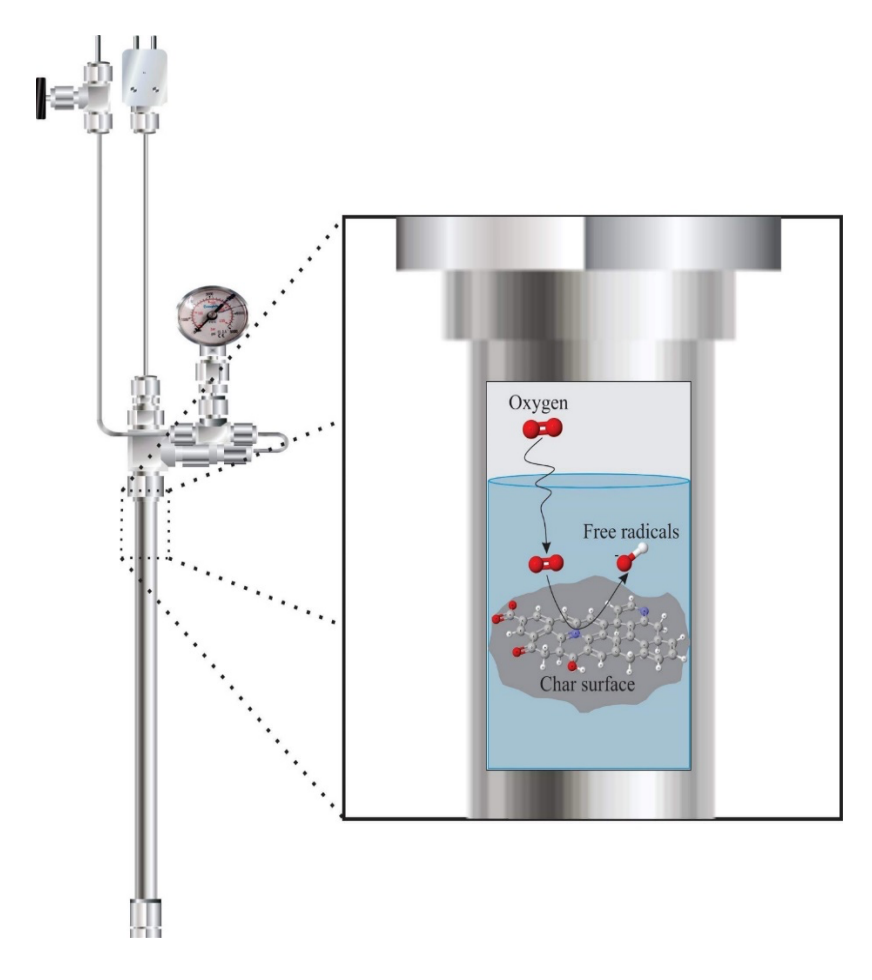


Figure 1SI. Hydroquinone production during phenol oxidation in stainless steel glass lined reactor at different temperatures.



**Figure 2SI.** Hydroquinone production during phenol oxidation in stainless steel glass lined reactor in the presence of 0.2 wt. % char catalyst.



**Figure 3SI.** Schematic of molecular oxygen reaction with nitrogen doped char to produce hydroxyl free radicals in the phenol oxidative system